The effect of impact-generated heterogeneities and discontinuities on the subsequent weathering of impactites: insights from laboratory experiments

Ankit Kumar Verma[1], Mary C Bourke[1], Heather A Viles[2], Gordon R Osinski[3], and Juan Diego Rodriguez-Blanco[1]

[1]Trinity College Dublin
[2]University of Oxford
[3]University of Western Ontario

November 24, 2022

Abstract

Impact cratering is an important geological process that affects all planetary bodies in our solar system. As rock breakdown plays a vital role in the evolution of landforms and sediments on a planetary scale, it is crucial to assess the role of inheritance in the subsequent breakdown of impactites (impact rocks). The shock pressure of several gigapascals generated during the impact can exceed the effective strength of target lithology by three to four orders of magnitude and is responsible for melting, vaporisation, shock metamorphism, pore collapse, vesiculation fracturing and fragmentation of rocks. Environmental conditions and heterogeneities in rock properties exert an important control in rock breakdown. Similar to other subaerial rocks, impactites are affected by a range of rock breakdown processes. In order to better understand the role of low-shock inheritance on rock breakdown, a rock breakdown experiment was conducted in a simulated environmental cabinet under conditions similar to terrestrial semi-arid conditions. We cycled temperature (-2 to 35°C) and relative humidity (13-45%) through 39 accelerated diurnal cycles (each of 8 hours duration). We used 41 impactite samples in the experiment that included low shocked sedimentary and crystalline rocks, impact melt rocks and impact breccias. Mechanical (Equotip and weighing), photographic (photographic monitoring), microscopic and solid-state methods (petrographic microscopy, powder X-ray diffraction, scanning electron microscopy, X-ray computed tomography) were used to characterise the rock samples relative to unshocked rocks, and to assess the shock related changes before and after the experiments. The low shocked sedimentary rocks showed a decrease in porosity by 38% (Coconino Sandstone) and 88% (Moenkopi Sandstone) compared to unshocked counterparts. Macrofractures of 0.1-0.2 mm and microfractures 0.1-5 μm in aperture were observed in all types of impactites. The results showed that impactites exhibited an accelerated decline in strength compared to non-impacted control samples. However, rock type and impact deformation history were key parameters controlling the rate of deterioration.

The effect of impact-generated heterogeneities and discontinuities on the subsequent weathering of impactites: insights from laboratory experiments

Ankit K. Verma[1], Mary C. Bourke[1], Heather A. Viles[2], Gordon R. Osinski[3], Juan Diego Rodriguez-Blanco[4]

[1]Department of Geography, Trinity College Dublin, The University of Dublin, Ireland,
[2]School of Geography and the Environment, University of Oxford, Oxford, United Kingdom,
[3]Centre for Planetary Science and Exploration, Department of Earth Sciences, University of Western Ontario, London, Ontario, Canada
[4]iCRAG, Department of Geology, Trinity College Dublin, The University of Dublin, Ireland

Abstract

Impact cratering is an important geological process that affects all planetary bodies in our solar system. As rock breakdown plays a vital role in the evolution of landforms and sediments on a planetary scale, it is crucial to assess the role of inheritance in the subsequent breakdown of impactites (impact rocks). The shock pressure of several gigapascals generated during the impact can exceed the effective strength of target lithology by three to four orders of magnitude and is responsible for melting, vaporisation, shock metamorphism, pore collapse, vesiculation fracturing and fragmentation of rocks. Environmental conditions and heterogeneities in rock properties exert an important control in rock breakdown. Similar to other subaerial rocks, impactites are affected by a range of rock breakdown processes. In order to better understand the role of low-shock inheritance on rock breakdown, a rock breakdown experiment was conducted in a simulated environmental cabinet under conditions similar to terrestrial semi-arid conditions. We cycled temperature (-2 to 35°C) and relative humidity (13-45%) through 39 accelerated diurnal cycles (each of 8 hours duration). We used 41 impactite samples in the experiment that included low shocked sedimentary and crystalline rocks, impact melt rocks and impact breccias. Mechanical (Equotip and weighing), photographic (photographic monitoring), microscopic and solid-state methods (petrographic microscopy, powder X-ray diffraction, scanning electron microscopy, X-ray computed tomography) were used to characterise the rock samples relative to unshocked rocks, and to assess the shock related changes before and after the experiments. The low shocked sedimentary rocks showed a decrease in porosity by 38% (Coconino Sandstone) and 88% (Moenkopi Sandstone) compared to unshocked counterparts. Macrofractures of 0.1-0.2 mm and microfractures 0.1-5 μm in aperture were observed in all types of impactites. The results showed that impactites exhibited

an accelerated decline in strength compared to non-impacted control samples. However, rock type and impact deformation history were key parameters controlling the rate of deterioration.

1. Introduction

Impact cratering is a ubiquitous and catastrophic geologic process that has a crucial role in the evolution and modification of all planetary bodies with solid surfaces. During impact, the energy released is much higher than any endogenic geological processes. During an impact event, the impact shock wave is translated into more intense shock-related deformation and melting of target rocks extensively beneath and around the impact crater compared to those located at a far distance (Kenkmann et al., 2014; Pierazzo and Melosh, 2000). In the case of porous rocks like sandstone, this effect is more pronounced (Kieffer, 1971b; Kieffer et al., 1976b).

A range of impactites such as shocked target rocks, impact melt rocks, impact breccias, impact melt-bearing breccias, and tektites are usually found at impact sites. Impactites are classified into autochthonous, parautochthonous and allochthonous based on origin and current location at the impact site. Allochthonous impactites are further classified into proximal and distal based on distance from the impact site. A detailed classification of impactites can be found in Stöffler et al. (2007) and Grieve and Therriault (2013).

During impact, porosity, permeability and density can dramatically change depending on the energy released and the target lithology as well as the distance from the point of impact (Cockell and Osinski, 2007; Kieffer, 1971b; Singleton et al., 2011). The impact metamorphism processes and their effects differ in non-porous crystalline target rocks in comparison to porous sedimentary rocks (Cockell and Osinski, 2007; Kieffer, 1971b; Osinski, 2007; Singleton et al., 2011; Stöffler et al., 2018).

In crystalline rocks, porosity increases with an increase in shock pressure levels (Singleton et al., 2011). This is caused due to fracturing and differential mineral melting during the passage of the shock and subsequent rarefaction wave (Singleton et al., 2011).

For porous sedimentary rocks, such as sandstone, that are subject to low shock pressure levels (<10 GPa) the rock density increases due to pore collapse, comminution and fracturing of grains. Rock density decreases as shock pressures rise ($25 > P > 10$ GPa) due to vesiculation and formation of glasses and melts that weld mineral grains (Kieffer, 1971a; Kieffer, 1971b).

At even higher shock pressures (>30 GPa) the porosity is further reduced as minerals recrystallise from the melt (Cockell and Osinski, 2007).

If impact rocks are subject to longer-term heating and annealing during crater cooling, the porosity and permeability will be affected further. For highly porous substrates (such as sandstones), more of the impact energy is taken up in pore collapse resulting in lesser solid state transformations and higher post-shock temperatures than a similar impact into non-porous crystalline target lithology (Kieffer, 1971b; Madden et al., 2006).

There are two shock-related features that we investigate in this study, micro-fracturing and mineral-scale deformation. First, The role of micro-fracturing as a control on the moisture flux in rocks is held to be important in subsequent rates of rock breakdown (Anders et al., 2014; Sousa et al., 2005). Impact fractures and microcracks, produced during impact, increase secondary porosity and affect the total porosity and permeability of the rocks. However, microfracturing is not well understood in any environment (Anders et al., 2014).

Second, naturally occurring distinct diagnostic mineral deformation features related to impact shock waves such as planer fractures, planar deformation features, feather features, toasting, mosaicism, kink bands, high-pressure mineral phase transformations and impact shock melting at various shock pressures are well documented in the literature (Ferrière and Osinski, 2013; French and Koeberl, 2010; Stöffler et al., 2018), and assigned shock pressure levels by calibrated laboratory experiment (Kieffer et al., 1976a; Kieffer, 1971b; Shipman et al., 1971). What has not been adequately investigated is the role of the mineral-scale deformation features may have on the subsequent breakdown of rocks.

1.1. Previous work

Environmental conditions and heterogeneities in rock properties exert an important control in rock breakdown. Earlier studies have demonstrated that pore geometry affects rock susceptibility to weathering and controls the intensity of weathering (Tuğrul, 2004). Several studies (Newsom et al., 2013; Wright, 2013) have reported a unique style of rock breakdown associated with decompression cracks in impacted basalt at Lonar Crater, India. Natural silicate glasses are susceptible to accelerated dissolution when compared to their crystalline counterparts (Wolff-Boenisch et al., 2006). Since, impact generated glasses have a different texture, density and structure (French and Koeberl, 2010), they may weather differently. The structural defects, deformations and change in surface area of minerals makes shocked rocks more susceptible to chemical weathering than unshocked rocks (Bell, 2017; Boslough and

Cygan, 1988). Moreover, microstructures and defects in minerals generated during impact shock (e.g. Planar Fractures (PFs), Planar Deformation Features (PDFs), mosaicism, microfractures) can provide permeable pathways for fluid circulation leading to chemical weathering (Furukawa et al., 2011; Leroux, 2005). Increasing shock pressures also causes devolatilization in minerals (Madden et al., 2006), which may affect the response of rocks to thermal weathering (Farquharson et al., 2017).

To understand the mechanism, style and rate of weathering and the role of a range of environmental factors, geomorphologists conduct weathering experiments in controlled laboratory conditions. A range of weathering and field exposure experiments has been conducted to understand the role of lithology (Viles and Goudie, 2007; Warke, 2007), environment and microclimate (e.g. Goudie and Parker (1998); Smith et al. (2011); Viles et al. (2010); Viles and Goudie (2007); Viles (2005); Warke and Smith (1998), mechanism and style of deterioration (De Kock et al., 2015; Ghobadi and Babazadeh, 2015; Williams and Robinson, 2001), the presence of salts (Goudie and Parker, 1998; Goudie et al., 2002; Smith et al., 2005; Warke, 2007), and porosity and fractures (Sousa et al., 2005; Tuğrul, 2004). These data have emphasised the role of stress history and the inherited weakness that may result from past weathering. Few studies used simulated pre-stressed rocks (sedimentary and crystalline) with different weathering histories and subjected rocks to experimental weathering and field exposure trials in arid conditions (Viles et al., 2010; Viles et al., 2018; Warke, 2007). They found that pre-stressed rocks deteriorate faster than un-stressed rocks. Moreover, the nature of pre-stressing had a significant effect on the rate of breakdown (Viles et al., 2010; Viles et al., 2018; Warke, 2007).

No detailed study has been undertaken to explore the role of impact metamorphism and the effect of inherited heterogeneities and deformation caused by impact process on subsequent on subsequent style and rate of weathering. Here, we present data from the first physical weathering experiment in simulated semi-arid conditions on impactites. The focus of this study is to identify how the inheritance of an impact event affects the subsequent breakdown of impactites exposed at the surface to sub-aerial weathering.

2. Materials and methods

2.1. Sample source

The primary focus of this study is to understand the effect of impact-related deformation on weathering of sandstone in simulated weathering environmental conditions using low-shocked sedimentary rocks sampled from Meteor Crater (USA). We also report on pilot weathering experiment on a small number of crystalline impacted rocks, impact melt rocks, and impact breccias from West Clear Water Impact Structure (Canada) and Ries Crater (Germany) as these are also common rocks in terrestrial impact craters, but they have a different impact history. Forty-one samples of impactites and non-impacted rocks were selected for the weathering experiment.

2.1.1. Meteor Crater Samples: Sedimentary impacted rocks

Two types of sedimentary rock samples are included in this study. These are Permian Coconino Sandstone, and Triassic Moenkopi Sandstone sampled from the 50, 000 years old 1.2 km diameter Barringer Meteorite Crater aka Meteor Crater in Arizona (Kieffer, 1971a; Shoemaker and Kieffer, 1979). The impacted samples were collected from NW, NE, SE and S Crater walls and the ejecta blanket on the south side of the crater. Non-impacted varieties of Coconino and Moenkopi Sandstone samples were included as control samples in the experiment. Non-impacted Moenkopi Sandstone samples were collected from two sites along Meteor Crater road that experience similar environmental conditions, 5 and 9 km from the Meteor Crater. Non-impacted Coconino Sandstone samples were collected from Clear creek reservoir 50 km from Meteor Crater (this was one of the closest surface exposures). Ten impacted Coconino sandstone, thirteen impacted Moenkopi sandstone and two non-impacted (control) samples of both Coconino and Moenkopi Sandstone were used in the weathering experiment (i.e., 27 samples). Impacted samples were named according to Barringer Crater Reference Collection naming convention (*pers. comm*. D. Kring).

2.1.2. West Clearwater Impact Structure samples: Crystalline impacted rocks, impact melt rocks, and impact breccias

The ~36 km diameter West Clearwater Impact Structure (WCIS) is about 125 km east of Hudson Bay in Quebec, Canada (Simonds et al., 1978). WCIS is ~286 Ma old and is relatively well preserved with a large ring of islands in the ~30 km diameter lake (Osinski and Grieve, 2017; Schmieder et al., 2015). The samples from this crater were collected during NASA FINESSE (Field Investigation to Enable Solar System Science and Exploration) expedition in

2014 by one of the co-authors. Target lithologies comprise granitic gneiss, granite, tonalite, granodiorite, quartz monzodiorite with later diabase dykes (Osinski and Grieve, 2017; Phinney et al., 1978; Rae et al., 2017; Rosa, 2012; Simonds et al., 1978). Osinski and Grieve (2017) proposed a general stratigraphy of impactites from the bottom to top in the sequence: Fractured basement > lithic impact breccia > impact melt-bearing breccia or suevite > clast rich impact melt rock > clast poor impact melt rock > clast free impact melt rock.

Impacted granite and tonalite samples were collected from around the rim and impact melt rocks and impact breccias were collected from ring islands. Samples were named according to NASA FINESSE WCIS campaign naming convention.

2.1.3. Ries Crater samples: Impact melt-bearing breccia or suevite

The ~26 km diameter Ries Crater in western Bavaria, Germany is one of the best preserved terrestrial mid-sized complex impact structures (Pohl et al., 1977). Ries crater was formed ~15 million years ago in the flat-lying sequence of Mesozoic sedimentary rocks that unconformably overlie Hercynian crystalline basement (Osinski, 2003; Pohl et al., 1977; Rocholl et al., 2018; Schmieder et al., 2018). A single Suevite sample from this crater is used in this study. The sample came from the repository collection of one of the co-authors, and its precise sample location in the field is not known.

2.2. Sample preparation

Polished thinsection of 30 μm thickness was prepared for petrographic examination. Powdered samples were prepared in a mortar and pestle for X-ray diffraction analysis. For the weathering experiments, rock samples were cut into cube blocks of 5 cm side length using a wet rock saw at Trinity College Dublin. A few samples which were not big enough for making 5 cm cube blocks, were cut down into the biggest dimension possible (see Table 1-4).

2.3. Characterisation of samples

Characterisation of samples was necessary to describe the deformation and changes in rock samples due to impact. Several laboratory analysis techniques were used to characterise petrographical properties in rock samples. Samples were assessed to determine compositional and textural properties using a combination of qualitative and quantitative techniques including

scanning electron microscopy (SEM), powder X-ray diffraction (XRD), petrographical microscopy and X-ray computed tomography (CT). In order to classify each sample into a shock pressure class, the shock deformation state of quartz was determined in polished thinsection under a petrographic microscope. These features were then matched to the published classification, and the shock pressure class was assigned to the samples (Kieffer, 1971b; Stöffler et al., 2018) based on the presence and absence of specific shock features (e.g. PF, PDFs) in quartz and decreasing quartz content in the samples due to conversion into high-pressure polymorphs and glass. Quantitative powder X-ray diffraction was used to determine the relative proportion of high-pressure mineral polymorphs in the samples. The shock progression seen in the quartz is similar to that found in other studies (Engelhardt, 1997; Kieffer, 1971b; Rae et al., 2017; Rosa, 2012).

2.3.1. Quantitative X-ray diffraction (XRD) for identification of mineral phases in rock samples

Quantitative powder X-ray diffraction (XRD) analysis was performed on rock sample to identify and measure relative proportion of minerals and their high-pressure polymorphs formed during impact using the Bruker D5000 in Trinity College Dublin and the Panalytical X'Pert Pro XRD at the Natural History Museum, London. These data allowed us to assign shock pressure class to these samples based on abundances of higher-pressure mineral polymorphs. Furthermore, powder XRD was used to identify salt species present in the field.

The Bruker D5000 in Trinity College Dublin has a 2.2 kW Cu long fine focus (0.4 x 12mm filament), with the following optical configuration: 2.5° primary soller, 1 mm aperture diaphragm, 1 mm scattered radiation diaphragm, no secondary soller, 0.2 mm detector diaphragm and a secondary curved graphite monochromator ahead of the scintillation counter. A scan of the sample was made from 5 to 70° 2θ at a speed of 2 seconds / 0.02° step at 40 kV and 40 mA. Sample rotation was used. This technique was used to determine the mineral composition and identify high-pressure polymorphs of quartz in the Moenkopi Sandstone. These data allowed us to assign shock pressure class to these samples based on abundances of higher-pressure mineral polymorphs. Rietveld refinement was used to determine the weight percentage of various mineral phases in the samples.

The Panalytical X'Pert Pro XRD at Natural History Museum, London was used to analyse Coconino sandstone, crystalline impactites, melt rocks and breccia samples. It has a primary monochromator and para-focussing optics for high-resolution measurements of Cu radiation,

with divergence slit 0.25, soller slits 0.02 rad, and an X'celerator solid-state detector. It used Bragg Brentano geometry. Data was collected from 3-120° 2θ with a step size of 0.017°, per step 100 s at 45 kV and 40 mA.

Identification of crystalline phases was carried out with the Philips X'pert HighScore software in combination with the Powder Data File (PDF-2, The International Centre for Diffraction Data (ICDD)). Pattern-matching refinement and quantification of percentage of crystalline phases in rock samples were carried out with the Rietveld refinement software TOPAS (Bruker and Topas, 2003).

2.3.2. Petrographic examination using scanning electron microscope (SEM) and petrographic microscope

A petrographic microscope and SEM were used to analyse and identify the composition and impact associated deformation features (e.g., PF, PDFs, microfractures) of the rock. Polished thin sections were examined under Nikon Eclipse LV100 petrographic microscope. Grain size and sorting analysis for sedimentary rocks were carried out by using the DSG-master Matlab tool developed by Buscombe (2013). A Zeiss Axio Imager 2 microscope was used to obtain mosaics of thin sections in order to understand the composition and clast-matrix relationship of the rocks.

A Tescan Mira XMU Field Emission scanning electron microscope (SEM) at the Centre for Microscopy Analysis (CMA) in Trinity College Dublin was used to obtain Backscattered Electron (BSE) images of rock thin sections. The SEM was equipped with KE Developments Centaurus system. Thin sections were carbon coated to a thickness of 10 nm to aid conductivity. BSE images were obtained at a working distance of 18 mm. Beam operating conditions were 20 kV of accelerating voltage and probe current of 10 pA.

SEM BSE mosaics (~50 mm^2) were used for porosity determination of impacted and non-impacted samples (Buhl et al., 2013). SEM BSE mosaics (~50 mm^2) represents significant subsection of the entire thinsection. The area for BSE mosaic was selected manually by locating subsection of thinsection that roughly represented the whole thinsection. Macrofractures were avoided in the field of view BSE mosaic for estimating primary porosity of rock sample in order to avoid any bias in the result. Porosity in rock samples was estimated by quantitative BSE image analysis in freely available software Image J following established methodology

(Buckman et al., 2017). BSE images have high contrast which enables discrimination between grains and the lowest intensity (or darkest) epoxy-filled pore spaces. Grey-Scale intensity thresholding was visually applied at the default setting by manually adjusting the intensity in order to capture the maximum degree of observed porosity. The percentage area of thresholded pore space was measured for porosity percentage determination. BSE images were also used to quantify the microfractures in rock samples.

2.3.3. X-ray computed tomography (CT)

X-ray CT was used to visualise and quantify macro-fractures (0.1 mm – 1 mm) present in the sample blocks. A Nikon Metrology HMX ST 225 X-ray CT at the Natural History Museum (London) was used to characterise the samples. X-ray CT images were acquired at 200 kV and 200 μA using 0.5 mm copper filter and ultra-focus X-ray head. Approximately 3142 projections were acquired at 2 frames per projection by 0.2 mm detector pixel size. The X-ray CT scanned 2 hours for each sample at 0.046 mm voxel size. The scan was reconstructed into a 16-bit unsigned raw file format which took 1.5 hours for each sample. The resolution of 0.046 mm per voxel is the highest that could be achieved for 5 cm cube rock block with this approach.

X-ray CT was used to characterise macro-fractures both before and after the environmental chamber experiments (De Kock et al., 2015). This technique helped to quantify the presence of pre-existing micro-fractures and those that may be enhanced or generated by the experiments.

2.4. Laboratory weathering experiment

2.4.1. Weathering experiment design

In order to understand the role of impact inheritance on rock weathering, an experiment was conducted to simulate physical weathering under terrestrial semi-arid conditions over a short timespan (c 39 diurnal cycles). A Sanyo Fissons-FE300H/MP/R20 environmental cabinet was used to simulate the semi-arid environment conditions found at Meteor Crater in Arizona during spring. It is required to ensure the samples have sufficient exposure to manifest a physical response to the conditions. Shorter run times may not produce measurable effects. Viles et al. (2010) ran terrestrial simulations for 12 days on basalt and had a successful outcome. Due to limited availibility of funding and access to the environmental cabinet facility, the experiment was run for 13 days.

In the physical weathering experiment, environmental cycling simulated heating and cooling, wetting and drying, freeze and thaw, and salt weathering processes. Our motivation was to simulate natural weathering conditions to produce an observable rock breakdown in the short experiment timeframe available. Forty-one sample blocks of impactites and non-impacted rocks were used in this experiment.

To provide a pedogenic component to the experimental environment and to isolate the base of the rock from the metallic tray, a ~2 cm thick sand layer was placed in sample trays (Fig 1). Building sand (quartz sand) was used in this experiment which had similar albedo and grain size as the sand found at Meteor Crater site. This was done to recreate field-like thermal gradients. The mean grain size of the sand used in the experiment was 270 μm (measured by Malvern Laser Particle Sizer Mastersizer 2000) which is similar to sand sampled from the field site (230 μm, measured by dry sieving). Salt samples (MC51417-3 and MC51417-4) collected in the field at the Meteor Crater site were analysed to identify the salt species. Gypsum salt (calcium sulphate dihydrate, $CaSO_4 \cdot 2H_2O$) was detected in the powder XRD analysis and was used in this experiment to simulate the natural field conditions. Although gypsum is not known to be an aggressive salt in short duration weathering experiment conditions (Charola et al., 2007; Williams and Robinson, 2001), gypsum salt was mixed into the sand in 1:10 ratio by weight as this sand to salt ratio is known to produce observable breakdown (Goudie and Parker, 1998; Goudie et al., 2002). The rock samples were placed on top of this sand-salt layer to simulate natural conditions in which salt uptake take place by a capillary rise in the field (Fig 1). Samples were separated in the tray to prevent possible interactions.

In this simulation, diurnal cycles of temperature and humidity (forced by convection) were accelerated so that each 24 hours was simulated over 8 hours in the environmental cabinet (Fig 1). Temperature and relative humidity data obtained from an iButton (Viles, 2011) deployed at Meteor Crater was used in this simulation. A full diurnal spring range (-2 to 35°C) which recorded the highest temperature gradient was chosen and compressed into an 8h cycle by reducing the length of time at near-constant temperatures to induce rock breakdown in reasonably realistic circumstances. This was done to preserve a natural rate of temperature change during periods of maximum heating and cooling and to minimise chamber time (Viles et al., 2010). An 8-hour cycle is appropriate as a shorter cycle require accelerating conditions too far from reality, that can have negative consequences on the experiment outcome. The mean rate of change in air temperature (dT/dt) in this experiment was ~0.15°C/min. Thirty-nine

cycles were repeated in total. Each cycle lasted 8 hours, and consist of 8 steps, of 1 h duration each step, with a constant cooling and warming rate. The temperature inside the environmental chamber was recorded using an iButton to ensure that the chamber was performing the temperature and relative humidity simulations correctly.

The chamber was configured into two compartments using a metallic shelf (Fig 1). Seven sample trays containing six samples in each tray were placed in the chamber (4 sample trays in the top compartment and 3 in the bottom compartment). A 40W halogen incandescent bulb was placed ~30 cm from the samples in each compartment of the chamber (Fig 1) to provide direct heating of rock surfaces by radiation to mimic natural condition of heat transfer (Viles et al., 2010; Warke and Smith, 1998). The lamp was switched on for half of each cycle using a programmable timer plug (Fig 1). The rain was simulated by spraying both the sand and the sandstone block surface with 25 mL of distilled water every 6 cycles. The spatial position of each sample tray was changed within chamber shelf sixth cycle when the chamber was opened for rain simulation to ensure equal exposure to any slight variations in conditions in the chamber (e.g. direct radiational heating variation due to the position of the lamp in the chamber). The surface temperature of the rock surface was monitored every sixth cycle with an infrared thermometer to ensure that rock does not get too much heat from an artificial light source.

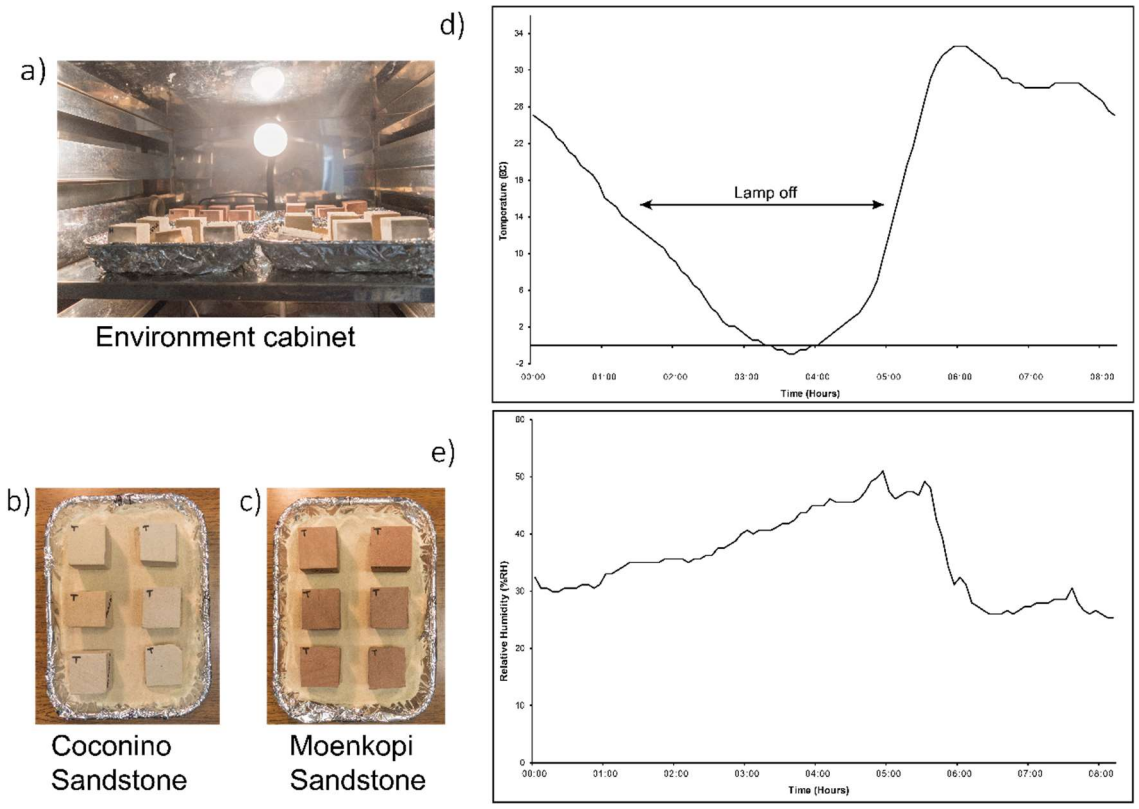

Fig 1. Physical weathering experiment protocols. (a) Terrestrial semi-arid condition simulation chamber with a lamp on top. (b) and (c) Rock sample tray. Sample blocks were placed on the sand-salt layer in the tray. (d) and (e) Temperature and humidity cycling of air in the simulation chamber.

2.4.2. Change metrics

Large-scale changes were monitored by weighing and photographing the samples before and after the experiments. Before weighing the sample at the end of the experiment, the samples were softly brushed to remove any sand, salt or debris attached to the rock surface. The change in weight is expressed as a percentage of initial block weight. A high-resolution Nikon D5500 24-megapixel camera with 35 mm prime lens was used to take scale photographs of the top and bottom facets of the sample blocks before and after the experiment. For small-scale changes, close up photographs of the rock samples were analysed before and after the rock breakdown experiments to identify and quantify changes in order to establish the nature, rate, and intensity of breakdown under experimental conditions.

Rock hardness was measured using the Proceq Equotip Piccolo Bambino 2 before and after the experiment to detect any changes in rock strength (Aoki and Matsukura, 2007; Kompatscher, 2004; Viles et al., 2011). The measurement was obtained using D device version (impact body 27 mm long, flat support ring) in HLD mode (Kompatscher, 2004). The hardness measured by

equotip are represented as Leeb hardness value (Kompatscher, 2004). Samples were supported by 1 m thick solid granite worktop bench. A rigid connection between the sample and solid support was ensured. The contact surface of the sample and the surface of the solid support was level, flat and smooth clean and dry. This was done to prevent unwanted energy absorption resulting in distortion in test results due to vibration as the impact body as the equotip hits the test point (Kompatscher, 2004). Twenty equotip measurements on each block were taken on different locations on the same surface and averaged. Any decrease in rock surface strength as a result of the generation of new microfractures or modification of an existing one is expected to be reflected in a decrease in Leeb hardness value (Aoki and Matsukura, 2007; Viles et al., 2011).

2.4.3. Desalination experiment

In order to quantify the amount of salt taken into macrofractures by capillary action during the experiment a series of desalination experiments were conducted. The samples were placed in individual, non-reactive, transparent, 1L cylindrical containers made up of Nalgene polypropylene copolymer material. The container was filled with 600 ml of distilled water, tightly capped and left for 48h. Samples were then removed and oven dried for 24 h at 50 °C to avoid the potential of inducing thermal breakdown. The experiment was repeated for three cycles. The conductivity of the water in which samples were immersed was measured using a handheld electrical conductivity meter and weight of the sample was recorded at the beginning and the end of each cycle. When there was little to no difference in the water conductivity or weight of the rock sample, then the experiment was stopped. At the end of the desalination, the sample strength was measured by Equotip. The Equotip measurement was carefully obtained on the same surface on which measurements were obtained before and after the weathering experiment. Care was taken to avoid previous Equotip measurement locations.

3. Results

3.1. Characterisation of rock samples

In this study, sedimentary and crystalline impactites samples were classified into shock pressure classes using XRD, SEM-BSE, and petrographic microscopy observation following

classification by (Kieffer, 1971a; Kieffer, 1971b; Madden et al., 2006; Stöffler et al., 2018). Below is a summary of the characterisation of impactite samples (Tables 1-4).

Table 1. Description of properties of Coconino Sandstone sample blocks used in the weathering experiment. Same sample names with Roman numerals in brackets indicate blocks cut from the same big sample.

Coconino Sandstone (CS)	Shock pressure class	Sample Size (cm)	Type of rock	Porosity (%)	Grain size (mm)	Sorting	Lamination	Visible macro-fracture in hand sample	Petrographic overview
MC51417-5 (I)	1A	~5×5×5	Ejecta	5.81	0.12	0.08	Five sets parallel lamination bands, the width of the band is 1 mm	No	**Class 1a (<5GPa) CS** may have experienced <5GPa of shock pressure during impact. In general, specimens of class 1a shocked CS do not differ in macroscopic appearance from unshocked CS. The grains are weakly to moderately cemented. In thin section, these rocks have less porosity than massive unshocked Coconino Sandstone. Porosity has been reduced in these samples due to compaction caused by slight translation and rotation of individual grains or small group of grains during the passage of shock waves. However, remnant porosity is still visible under a petrographic microscope. Less than 5% of quartz grains show wavy extinction under cross-polars. Class 1a samples retain their original grain size as in found in unshocked samples and 37-65% quartz grains displayed irregular microfractures (Madden et al., 2006).
MC51417-5 (II)	1A	~5×5×5	Ejecta	5.81	0.12	0.08	5 sets parallel lamination bands, width of band is 1 mm	No	
MC51417-6	1A	~5×5×5	Ejecta	14.42	0.09	0.07	No, massive	No	
MC51417-7	1A	~5×5×5	Ejecta	18.5	0.14	0.09	8 bands of width 1 mm parallel, closely spaced 0.5 cm	No	
MC51417-8	1A	~5×4×4	Ejecta	12.27	0.09	0.06	No, massive	No, crumbled corner	
MC51517-2	1A	~5×5×3	Crater wall rock	12.72	0.11	0.07	Four bands of lamination with 1 mm width, closely spaced 0.5 cm	One set of fracture 3 cm in length and 0.2 cm in width only visible on two adjacent surfaces, broke along a fracture or lamination during sample preparation	
MC51517-4	1A	~5×5×5	Crater wall rock	13.69	0.12	0.08	No, massive	One set of fracture 4 cm in length and 0.2 mm width only visible on two adjacent surfaces	
MC51517-8 (I)	1A	~5×5×5	Crater wall rock	13.69	0.16	0.09	No, massive	One set of fracture,5.5 cm in length, 0.2 mm wide, visible only on two adjacent surfaces of the block	
MC51517-8 (II)	1A	~5×5×5	Crater wall rock	13.69	0.16	0.09	One band of ~1 mm thick lamination, massive	No	
MC51417-9	1B	~7×7×3	Ejecta from quary	10.98	0.1	0.07	no, but the friable sample	No	**Class 1b (~5 GPa) CS** is fragile and friable, fine-grained, powdery in texture. The rock is snow white in hand sample and can be broken by gentle hand pressure. The size of the grains is reduced by fracturing, only a fraction of the grains preserves the original grain size. These isolated grains are surrounded by much smaller, highly fractured quartz particles. In class 1b CS ~98% of grains contain irregular fractures (Madden et al., 2006). The aperture/width of intragranular microfracture in the quartz grains in low shocked Coconino Sandstone ranged from 0.1-5 um.
CLR-1	unshocked	~5×5×5	Control	20.44	0.09	0.07	No, massive	1.5 cm long fracture, visible on two adjacent surfaces only.	**The unshocked CS** is pale buff, white, fine-grained, saccharoidal, cross-bedded eolian Sandstone Detrital quartz grains in the sandstone are generally well rounded, well sorted. CS contains 94-99 % quartz 0.4 – 5 % kaolinite, and minor feldspar, heavy minerals (rutile, zircon), calcite and hematite as secondary deposits can occur in trace quantity.
CLR-2	unshocked	~5×5×5	Control	20.93	0.09	0.04	No, massive	No	

Table 2. Description of properties of Moenkopi Sandstone sample blocks used in the weathering experiment. Same sample names with Roman numerals in brackets indicate blocks cut from the same big sample.

Moenkopi Sandstone (MS)	Shock Pressure class	Sample Size (cm)	Type of rock	Porosity (%)	Grain size (mm)	Sorting	Lamination	Visible macrofracture in Hand sample	Petrographic overview
MC8215-01	1A	~5×5×3	Crater wall rock	0.7	0.09	0.06	No, massive	Two sets of fractures passing through two facets, the first one is 2 cm in length and the second is 6 cm long. The aperture of the fractures is 0.1 mm	**Class 1a (<5GPa) MS** may have experienced <5GPa of shock pressure during impact. In hand specimen, there is no visible difference between class 1a and unshocked MS. No high-pressure polymorphs were identified in XRD analysis and no change in mineralogy was observed in class 1a MS compared to unshocked MS. Macroscopic fractures are present in some of the class 1a MS samples. Due to low shock, this porosity is reduced in class 1a MS. The porosity in low, shocked Moenkopi is 0.5-1%. No irregular grain fracturing due to impact can be seen in class 1a MS. A small amount of the quartz grains shows wavy extinction
MC51317-1	1A	~5×5×5	Crater wall rock	0.58	0.09	0.06	Three sets of sub-parallel cross-laminations	No	
MC51317-2	1A	~5×5×5	Crater wall rock	0.78	0.09	0.06	Three sets of sub-parallel cross-lamination	Six set of fracture along cross-lamination on different facets. the length of fracture ranges from 1-2 cm and aperture 0.1 mm	
MC51317-03	1A	~5×5×5	Crater wall rock	0.50	0.1	0.06	No, massive	No	
MC51317-4 (I)	1A	~5×5×5	Crater wall rock	1.09	0.1	0.07	Three sets of sub-parallel cross laminations	One big 5 cm long and 0.2 mm wide orthogonal fracture visible on all facets. Smaller fractures are ranging from 1-2 cm long 0.1 mm wide visible on multiple facets.	
MC51317-4 (II)	1A	~5×5×3	Crater wall rock	1.09	0.1	0.07	Two sets of sub-parallel cross-laminations	Three sets of fracture ranging from 1.5-5 cm and aperture 0.1-0.2 mm visible on three facets	
MC51317-5	1A	~5×5×5	Ejecta	0.74	0.09	0.07	Four set of sub-parallel cross lamination	No	
MC51317-6	1A	~5×4×5	Ejecta	0.83	0.09	0.07	No, massive	One set of 4 cm long fracture visible on two adjacent facets. the aperture of the fracture is 0.1 mm	
MC51417-1 (I)	1A	~5×5×5	Crater wall rock	0.96	0.09	0.05	Three set of sub-parallel cross lamination	No	
MC51417-1 (II)	1A	~5×5×4.5	Crater wall rock	0.96	0.09	0.05	One set of visible cross lamination	Two set of small fractures on two adjacent faces, ranging in length from 1-2.5 cm and aperture 0.1 mm	
MC51417-2 (I)	1A	~5×5×5	Ejecta	0.71	0.07	0.05	Three sets of sub-parallel cross-laminations	No	
MC51417-2 (II)	1A	~5×5×5	Ejecta	0.71	0.07	0.05	One set of cross-lamination	No	
MC51417-2 (III)	1A	~5×5×2.5	Crater wall rock	0.71	0.07	0.05	Three sets of sub-parallel cross-laminations	No	

CS16-01	Unshocked	~5×5×5	Control	8.39	0.1	0.06	No, massive	No	**Unshocked Moenkopi** sandstone is very fine-grained sandstone which is cemented by carbonates. Moenkopi contains 50-80 % quartz, microcline, muscovite, hematite and kaolinite in minor amounts and remainder being composed of carbonate minerals (calcite and dolomite). Quartz is subrounded, equant, and well sorted and has subhedral grain boundary. The matrix is very fine grained and iron rich. The mean grain size ranges from 0.07-0.1 mm. The grain size ranges from 0.009-0.12 mm. The texture of the rock is grain supported.
CS16-02	Unshocked	~5×5×5	Control	5.23	0.08	0.06	Four set of sub-parallel cross lamination	No	

Table 3. Description of properties of crystalline impactite sample blocks used in the weathering experiment.

WCIS target rocks	Shock pressure class	Sample Size (cm)	Type of rock	Porosity (%)	Visible macrofracture in Hand sample	Petrographic overview
WCIS-14 MK-004	1a	~5×5×5	Target rock from around rim (granite)	0.07	Multiple macro-fractures on all surfaces ranging in length from 2-5 cm and 0.1 mm in aperture	**Class 1a granite (<10 GPa)** may have experienced <10 GPa shock pressure during impact. The granite sample has a pinkish grey hue in hand sample. Class 1a granite is medium grained hypidiomorphic, equigranular, with average grain-sizes varying from ~1 mm to up to ~3 mm. The granite samples contain quartz, albite, microcline and in minor amounts muscovite and clinochlore. Intragranular and intergranular fracturing is pervasive in the sample. Planar Fracture is present in quartz grains.
WCIS-14 MK-001a	1a	~3.5×3.5×3	Target rock from around rim (granite)	Negligible	One set of fracture 4 cm in length and 0.1 mm width only visible on two adjacent surfaces	
WCIS-14 Oz-015	1a	~4×3×3	Target rock from around rim (Tonalite)	0.26	No	**Class 1a tonalite (<10 GPa)** have undergone low shock (<10 GPa) deformation during impact. The sample looks greenish in hand sample. Class 1a tonalite is medium grained hypidiomorphic, equigranular, with average grain-sizes varying from ~ 1mm to up to ~3 mm. Class 1a tonalite contains quartz, albite, biotite, hornblende and in minor amounts calcite and clinochlore. Intragranular fracturing is pervasive in the sample. Kink bands can be observed in biotite. Planar Fractures in quartz is present.

Table 4. Description of properties of impact melt rock and impact breccia sample blocks used in the weathering experiment. Same sample names with Roman numerals in brackets indicate blocks cut from the same big sample.

Impactites	Sample Size (cm)	Type of rock	Porosity (%)	Visible macrofracture in Hand sample	Petrographic overview
WCIS-14 RW-019	~3.5×3.5×3.5	Clast rich fine-grained impact melt rock	2.91	No	This sample is massive and appears reddish-purple colour in hand sample due to oxidation of matrix. Clast rich melt rocks contain up to 25% fragments coarser than 1 mm. Clast rich impact melt rock contain quartz, andesine, sanidine, and minor muscovite, hematite and montmorillonite. Clasts usually compose 40-60%, and matrix occupies 60-40% of most of the samples (Rosa, 2012). The matrix is composed microlites made of iron oxide and plagioclase (<10 µm). The matrix has reacted with embedded clasts in clast rich impact melt rock. Clasts in the sample have micro-fractures.
WCIS-14 MK-082	~5×5×3	Clast poor fine-grained impact-melt rock	0.15	Multiple macro-fractures on all surfaces ranging in length from 1-5 cm and 0.1 mm in aperture	The clast poor impact melt rocks WCIS-14 MK-015, and WCIS-14 MK-087 appears red to purple in hand sample. Whereas, WCIS-14 MK-082 looks yellowish brown in hand sample. Clast poor impact melt rock contains less than 15% clasts larger than 1 mm across (Simonds et al., 1978, Rosa, 2012). Clast poor impact melt rocks WCIS-14 MK-015, and WCIS-14 MK-087 contain microcline, muscovite, andesine, and montmorillonite in minor quantity. Sample WCIS-14 MK-082 consist of quartz, anorthite, albite, sanidine and minor amounts of montmorillonite. In thin section, WCIS-14 MK-082 appears very different than WCIS-14 MK-015 and WCIS-14 MK-087. The melt matrix (size< 50 µm) in WCIS-14 MK-082 displays interlocking texture, whereas in WCIS-14 MK-015 and WCIS-14 MK-087 matrix displays fine-grained microlites (<10 µm) feldspar. Clasts in all clast poor impact melt rocks are fractured and reacted with the surrounding melt matrix. The matrix is oxidised in the samples. WCIS-14 MK-082 appears to be extensively chemically weathered/altered. WCIS-14 MK-015 may have been affected by hydrothermal alteration as it contains quartz vugs.
WCIS-14 MK-015	~5×5×3	Clast poor fine-grained impact melt rock	0.28	Multiple macro-fractures are ranging from 3-5 cm and 0.1 mm in aperture visible on multiple facets/ surfaces. Two vugs of diameter 0.5 and 1 cm are visible on two facets.	
WCIS-14 MK-087	~3×3×3	Clast poor fine-grained impact-melt rock	0.61	A few fractures ranging in length 1-2 cm with aperture less than 0.1 mm seen on three facets.	
WCIS-14 MK-60	~4×4×4	Clast free impact melt rock	1.51	One fracture 3 cm in length and 0.1 mm visible on one surface only	These samples contain no clast upto the size of 1 mm. These samples appear reddish brown in hand sample. They appear to be more coherent than clast rich- and clast poor- impact melt rocks. These samples contain quartz, anorthite, albite, muscovite, hornblende and minor montmorillonite. The matrix is oxidised and consist of devitrified glass. At high magnification, plagioclase laths (<10 µm) in matrix show interstitial texture. Clasts are fractured and have reacted to melt matrix.
WCIS-14 MK-077	~5×4×3	Clast free impact melt rock	0.21	No	
WCIS-14 MK-058B	~5×5×3	Lithic breccia	2.07	No	Lithic breccia appears red in hand sample. These samples contain larger clast (≥1 mm) embedded in the clastic matrix. The breccia samples consist of quartz, albite, orthoclase, muscovite, montmorillonite and minor hematite. The clasts are fractured and contain shock features. Toasted quartz and PDFs and PFs was observed in quartz and feldspar. In the thin section, matrix appears reddish brown due to oxidation.
WCIS-14 058C	~4×4×4	Lithic breccia	2.57	One set of fracture 4 cm in length and 0.1 mm in	

				aperture visible on only one facet	
WCIS-14 Oz-005	~5×5×3	Impact melt-bearing breccia or suevite	3.46	Multiple small fractures of length 1.5 cm and aperture 0.1mm visible three facets	WCIS-14 Oz-005 contain red, oxidised impact melt particles set in a fine-grained matrix. Glass component is surrounded by clastic groundmass (Osinski and Grieve, 2017). It contains clasts of quartz, feldspar. The clasts range in size from 100-900 micron. Hematite was present as opaque minerals. Some of the feldspar clasts are altered. Quartz clasts were fractured. The microfractures range from 0.1 to 4 microns in width. The glass fragment contains vesicles.
Suevite (I)	~5×5×5	Impact melt-bearing breccia or suevite	10.39	Multiple macro-fractures on all surfaces ranging in length from 1-5 cm and 0.1-0.2 mm in an aperture on all facets of the rocks.	Suevite samples contain clasts of vitric or glassy material, quartz, albite, microcline, hornblende, and minor amounts of muscovite and prehnite. Mineral clasts are 100-700 micron in diameter. The clast and lithic fragments are supported by clastic groundmass which forms up to ~80 % of the volume of which 30-50 % is glass (Osinski et al., 2004). All the mineral clasts are highly fractured, planar fractures were observed in some quartz grains, but most of the clast do not contain high-pressure shock features. The microfractures were 0.5-6 micron in width. Some of the mineral grains are appearing to be weathered. The samples contained macro-fractures in hand sample with aperture 0.2-0.4 mm and up to 2-5 cm in length.
Suevite (II)	~5×5×5	Impact melt-bearing breccia or suevite	10.39	Multiple macro-fractures on all surfaces ranging in length from 1-5 cm and 0.1-0.2 mm in the aperture. In hand sample observation, this sample contains more fractures and vitreous phases compared to Suevite (I)	

3.2. Experimental results

Figure 1 d and e show that our experimental design was successful in reproducing air and relative humidity changes known in semi-arid terrestrial conditions. At low temperatures (-2 to 5°C), a layer of dew was observed to precipitate on the top surface of the blocks. A gypsum salt crust was noted on the sand layer following water spray. At the end of the experiment, salt efflorescence can be seen on the surface of the blocks in contact with the sand-salt bed. In the following section, results from different types of impactites used in the weathering experiments are reported separately.

3.2.1. Sedimentary impactites

3.2.1.1. Coconino Sandstone (CS)

Table 5. Summary of results from weathering and desalination experiment

Coconino Sandstone	Shock pressure class	Equotip Leeb values before the experiment	Equotip Leeb values after the experiment	% change in Leeb values due to experiment	Equotip Leeb values after desalination	% change in Leeb values due to desalination	Conductivity (µS/cm)	%change in weight due to weathering experiment	%change in weight due to desalination
MC51417-5 (I)	1A	418	383	-8.37%	388	-7.18%	58	-0.12%	-0.07%
MC51417-5 (II)	1A	373	334	-10.46%	334	-10.46%	63	-0.09%	-0.07%
MC51417-6	1A	379	326	-13.98%	345	-8.97%	25	-0.06%	-0.05%
MC51417-7	1A	343	322	-6.12%	331	-3.50%	65	-0.08%	-0.07%
MC51417-8	1A	303	270	-10.89%	285	-5.94%	42	-0.07%	-0.06%
MC51417-9	1B	not measured	not measured	-	not measured	-	81	-0.45%	-0.23%
MC51517-2	1A	393	342	-12.98%	351	-10.69%	78	-7.42%	-0.09%
MC51517-4	1A	345	289	-16.23%	322	-6.67%	43	-0.07%	-0.03%
MC51517-8 (I)	1A	430	399	-7.21%	397	-7.67%	18	-0.05%	-0.04%

MC51517-8 (II)	1A	427	406	-4.92%	397	-7.03%	20	-0.04%	-0.03%
CLR-1	unshocked	386	363	-5.96%	355	-8.03%	31	-0.09%	-0.05%
CLR-2	unshocked	373	357	-4.29%	349	-6.43%	21	-0.10%	-0.05%
Mean percent change	**1A**			**-10.13%**		**-7.57%**		**-0.89%**	**-0.06%**
Mean percent change	**1B**			**not measured**		**not measured**		**-0.45%**	**-0.23%**
Mean percent change	**unshocked**			**-5.13%**		**-7.23%**		**-0.10%**	**-0.05%**

Most of the low shocked CS, assigned to shock pressure class 1a (Table 1) exhibited a higher loss in Leeb hardness values compared to unshocked CS following the weathering experiment (Fig 2). In terms of weight loss class 1a CS did not show any significant difference compared to unshocked rocks during weathering and desalination experiment (Fig 3). Sample MC51517-2 was the exception with the most significant amount of breakdown and debris (Fig 3). After desalination experiment class 1a CS (with the exception of MC51517-8 (I) and MC51517-8 (II)) gained strength whereas unshocked CS samples lost strength (Fig 2).

CS sample (MC51417-9) the only sample representing class 1b shock pressure class show a much more significant loss in weight in comparison to its unshocked counterpart during weathering and desalination experiment (Fig 3). This sample was not tested for rock strength using equotip as it was friable and start breaking with slight hand pressure.

Most of the class 1a and the sample 1b CS showed higher conductivity during desalination experiment (Table 5). The higher conductivity showed no correlation to higher porosity. X-ray CT examination did not reveal any new fracture growth or change in existing fracture aperture and length due to weathering experiment.

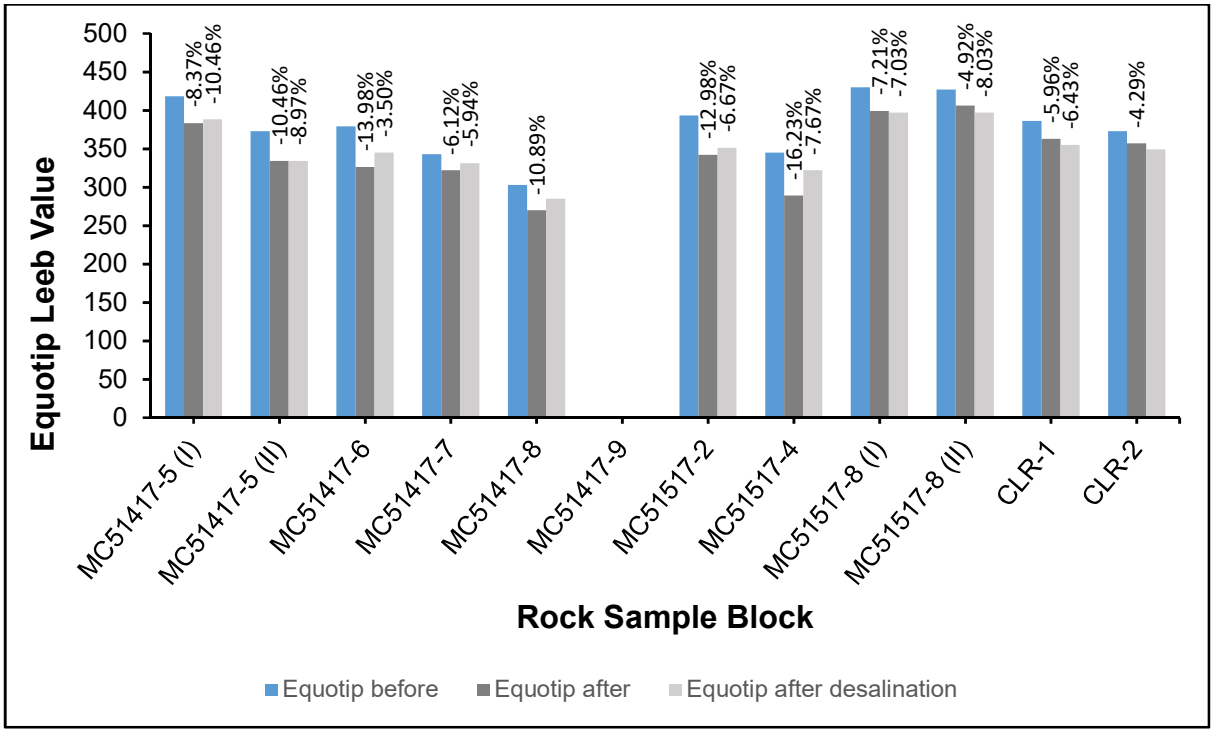

Fig 2. Change in Equotip Leeb Hardness value in Coconino Sandstone shock class 1a samples due to the weathering and desalination experiment. The percent value on top of each column is the percent change from the initial Leeb value. Equotip measurements were not obtained for shock class 1b sample MC51417-9 because it was friable.

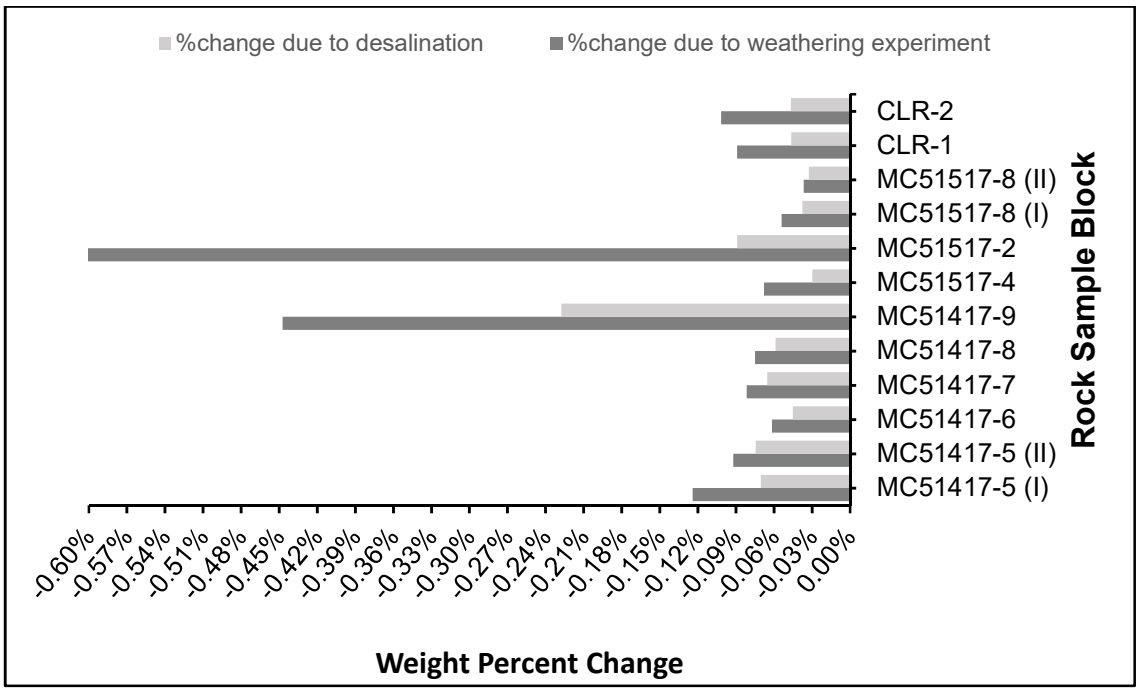

Fig 3. Percent weight change in Coconino Sandstone samples due to the weathering and desalination experiment (including shock class 1b sample MC51417-9).

3.2.1.2. Moenkopi Sandstone (MS)

Table 6. Summary of results from weathering and desalination experiment

Moenkopi Sandstone	Shock Pressure class	Equotip Leeb values before the experiment	Equotip Leeb values after the experiment	% change in Leeb values due to experiment	Equotip Leeb values after desalination	% change in Leeb values due to desalination	Conductivity (µS/cm)	%change in weight due to weathering experiment	%change in weight due to desalination
MC8215-01	1A	461	435	-5.64%	430	-6.72%	103	0.02%	-0.25%
MC51317-1	1A	485	470	-3.09%	464	-4.33%	102	0.20%	-0.16%
MC51317-2	1A	485	466	-3.92%	462	-4.74%	188	0.30%	-0.05%
MC51317-03	1A	489	461	-5.73%	458	-6.34%	80	-0.05%	-0.19%
MC51317-4 (I)	1A	450	449	-0.22%	429	-4.67%	186	0.23%	-0.21%
MC51317-4 (II)	1A	472	462	-2.12%	437	-7.42%	104	-0.07%	-0.21%
MC51317-5	1A	515	490	-4.85%	488	-5.24%	74	-0.01%	-0.17%
MC51317-6	1A	460	433	-5.87%	420	-8.70%	84	0.63%	-0.19%
MC51417-1 (I)	1A	451	432	-4.21%	430	-4.66%	87	-0.08%	-0.12%
MC51417-1 (II)	1A	432	423	-2.08%	398	-7.87%	63	0.19%	-0.12%
MC51417-2 (I)	1A	484	458	-5.37%	462	-4.55%	78	0.07%	-0.13%
MC51417-2 (II)	1A	501	479	-4.39%	473	-5.59%	92	0.02%	-0.13%
MC51417-2 (III)	1A	470	447	-4.89%	443	-5.74%	56	0.14%	-0.13%
CS16-01	unshocked	451	419	-7.10%	418	-7.32%	70	-0.06%	-0.12%
CS16-02	unshocked	503	474	-5.77%	474	-5.77%	70	0.03%	-0.15%
Mean	**1A**			**-4.03%**		**-5.89%**		**0.12%**	**-0.16%**
Mean	**unshocked**			**-6.44%**		**-6.55%**		**-0.02%**	**-0.14%**

All of the low shocked Moenkopi sandstone samples belong to class 1a. In these samples, primary porosity is reduced to ≤1% from ~5-8% in unshocked samples (Table 2). Some class 1a samples contain macroscopic fractures visible in hand samples (Table 2). Class 1a low shocked MS samples with no visible macro-fractures showed a similar loss in Leeb hardness to unshocked control samples due to weathering and desalination experiment (Fig 4). Class 1a MS samples with visible macro-fractures on the bottom surface in hand samples exhibited lower change Leeb hardness compared to unshocked control and other class 1a MS samples (Fig 4 and Table 2). The macro-fractures on the bottom surface (surface in contact with the sand-salt surface) in class 1a assisted in salt uptake due to capillary action which likely increased strength. These samples gained weight due to salt uptake might be higher than the loss of weight due to granular disintegration (Fig 5). In addition, the first conductivity measurement of the water containing these samples had higher conductivity values in comparison with unshocked control counterparts (Table 6). After desalination experiment, all the Class 1a MS samples lost strength as the salts were removed from the fractures. Unshocked

control samples showed very little to no change (Fig 4). After desalination experiment, all the class 1a samples which initially gained weight during the weathering experiment had lost weight (Fig 5). Of note is that Class 1a MS containing macro-fractures showed a higher decrease in strength after desalination compared to unshocked and other class 1a MS (Fig 4 and Table 2).

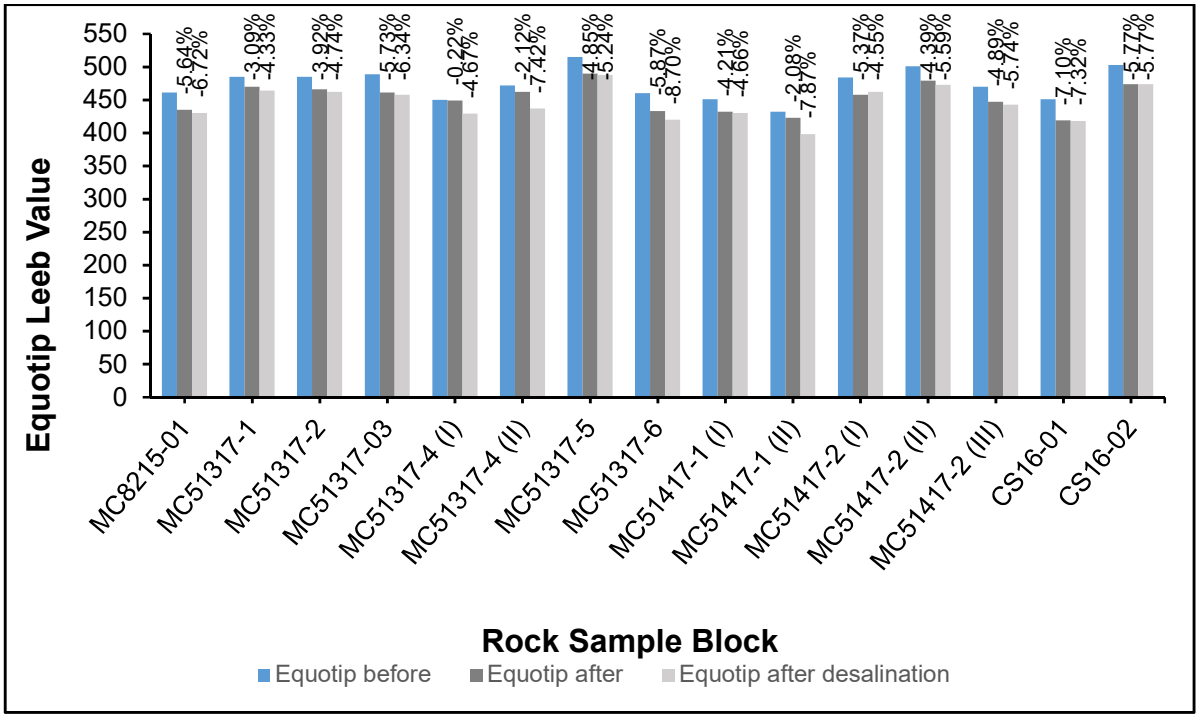

Fig 4. Change in Equotip Leeb Hardness value in Moenkopi Sandstone samples due to the weathering and desalination experiment. The percent value on top of each column is the percent change from the initial Leeb value.

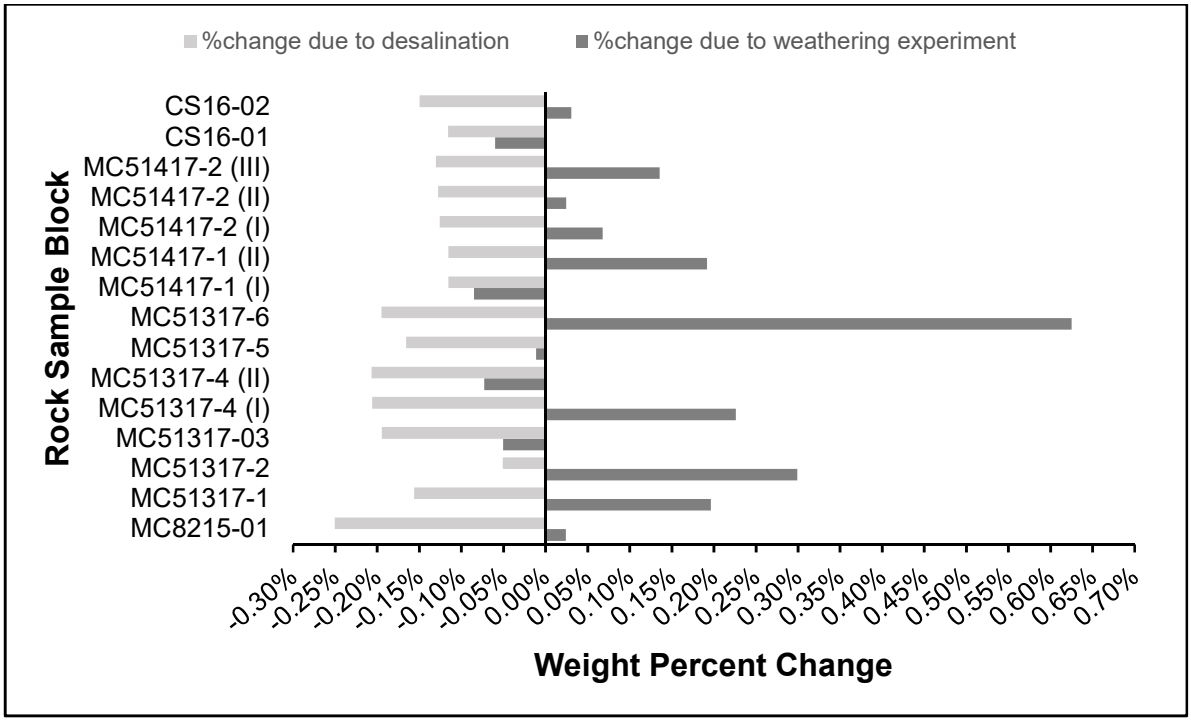

Fig 5. Percent weight change in Moenkopi Sandstone samples due to the weathering and desalination experiment.

3.2.2. Crystalline Impactites

Table 7. Summary of results from weathering and desalination experiment

WCIS target rocks	Shock pressure class	Equotip Leeb values before the experiment	Equotip Leeb values after the experiment	% change in Leeb values due to experiment	Equotip Leeb values after desalination	% change in Leeb values due to desalination	Conductivity (µS/cm)	%change in weight due to weathering experiment	%change in weight due to desalination
WCIS-14 MK-004	1a	855	835	-2.34%	824	-3.63%	22	0.00%	-0.03%
WCIS-14 MK-001a	1a	733	685	-6.55%	656	-10.50%	20	0.01%	-0.06%
WCIS-14 Oz-015	1a	710	708	-0.28%	658	-7.32%	16	0.01%	-0.04%

Two samples of low shocked granite and one sample of low shocked tonalite were used in the weathering experiment of crystalline impactites. These samples belonged to shock pressure class 1a. These rocks did not have an unshocked control counterpart.

Class 1a tonalite sample (WCIS-14 Oz-015) showed minimal change in strength due to weathering experiment but showed a higher change in strength following desalination (Fig 6). Class 1a granite samples (WCIS-14 MK-001a and WCIS-14 MK-004) exhibited a higher change in Leeb hardness compared to tonalite (Fig 6). The variation between granite samples may be due to impact-induced deformation heterogeneity. All samples showed a lowering of

Leeb hardness following desalination (Fig 6). While there was negligible weight loss due to weathering experiment or desalination (Fig 7). No visible granular fragments were observed, and X-ray CT examination did not show any new fracture growth or change in existing fracture aperture and length.

Shocked crystalline rocks have higher initial Leeb hardness compared to sedimentary impactites that represent the higher strength of crystalline rocks (Table 5-7). After desalination experiment class 1a granite and tonalite samples (WCIS-14 MK-001a and WCIS-14 Oz-015) showed a higher change in strength compared to unshocked Moenkopi and Coconino Sandstone samples, and most of the low-shocked Moenkopi sandstone (Table 5-7 and Fig 2, 4, and 6).

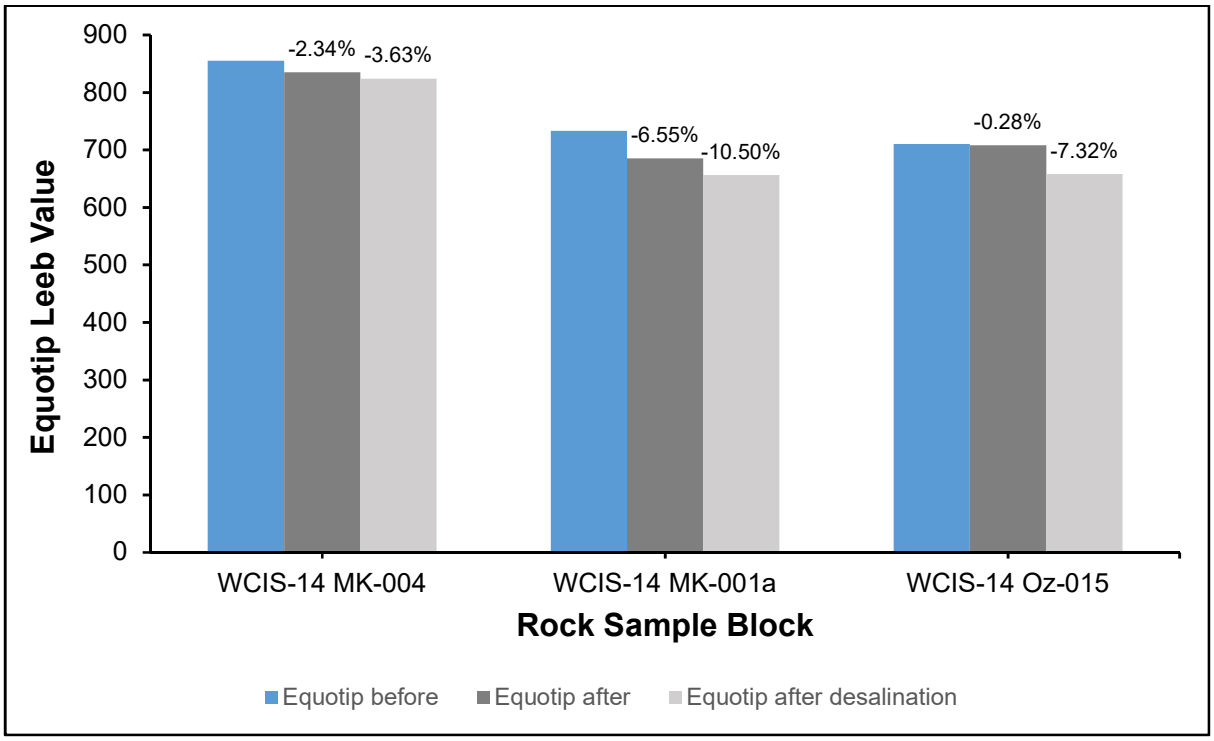

Fig 6. Change in Equotip Leeb Hardness value in crystalline impactites samples due to the weathering and desalination experiment. The percent value on top of each column is the percent change from the initial Leeb value.

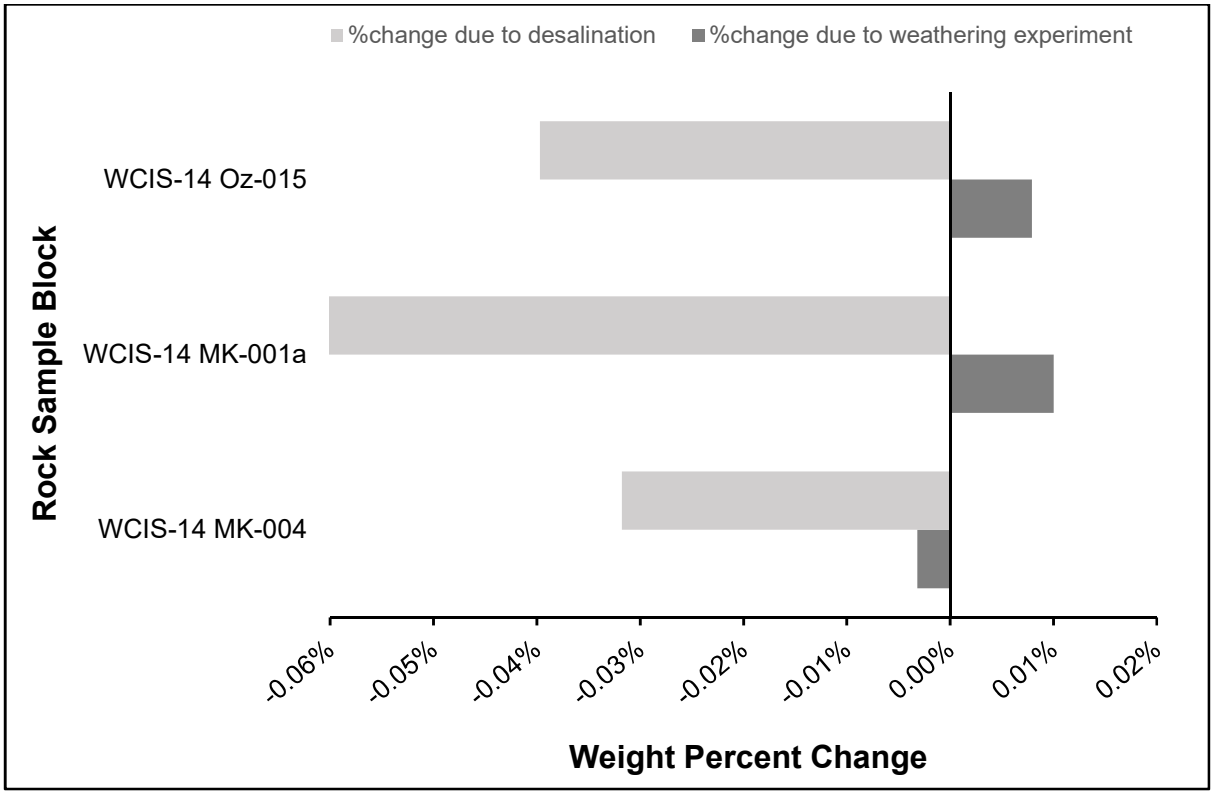

Fig 7. Percent weight change in crystalline impactite samples due to the weathering and desalination experiment.

3.2.3. Impact melt rocks and impact breccias

Table 8. Summary of results from weathering and desalination experiment

Impactites	Type of rock	Equotip Leeb values before the experiment	Equotip Leeb values after the experiment	% change in Leeb values due to experiment	Equotip Leeb values after desalination	% change in Leeb values due to desalination	Conductivity (µS/cm)	%change in weight due to weathering experiment	%change in weight due to desalination
WCIS-14 RW-019	Clast rich fine-grained impact melt rock	643	654	1.71%	578	-10.11%	16	-0.26%	-0.21%
WCIS-14 MK-082	Clast poor fine grained impact-melt rock	603	529	-12.27%	494	-18.08%	27	0.71%	-0.13%
WCIS-14 MK-015	Clast poor fine-grained impact melt rock	730	711	-2.60%	703	-3.70%	16	0.01%	-0.11%
WCIS-14 MK-087	Clast poor fine grained impact-melt rock	642	637	-0.78%	599	-6.70%	7	-0.17%	-0.43%
WCIS-14 MK-60	Clast free impact melt rock	769	740	-3.77%	723	-5.98%	15	-0.15%	-0.11%

WCIS-14 MK-077	Clast free impact melt rock	772	742	-3.89%	729	-5.57%	13	-0.02%	0.00%
WCIS-14 MK-058B	Lithic breccia	623	533	-14.45%	585	-6.10%	21	-0.13%	-0.08%
WCIS-14 058C	Lithic breccia	513	490	-4.48%	483	-5.85%	17	-0.04%	-0.82%
WCIS-14 Oz-005	Impact melt bearing breccia or suevite	476	402	-15.55%	404	-15.13%	27	-0.33%	-0.61%
Suevite (I)	Impact melt bearing breccia or suevite	321	327	1.87%	312	-2.80%	61	1.45%	-1.11%
Suevite (II)	Impact melt bearing breccia or suevite	394	351	-10.91%	324	-17.77%	53	2.01%	-1.28%

3.2.3.1. Clast rich fine-grained impact-melt rock

WCIS-14 RW-019 is a clast rich impact melt rock. The sample had an initial Leeb value lower than shocked crystalline impactites (Table 7-8). RW-019 showed a gain in strength during weathering experiment possibly due to salt uptake (Fig 8). After desalination experiment, the sample lost strength (Fig 8). This sample lost 0.26% in weight during weathering experiment (Fig 9). The sample may have lost more weight due to granular disintegration than gained weight due to salt uptake. The sample shows a slight loss in weight after the desalination (Fig 9).

3.2.3.2. Clast poor fine-grained impact-melt rock

WCIS-14 MK-015, WCIS-14 MK-087 and WCIS-14 MK-082 are clast poor fine-grained impact melt rocks. WCIS-14 MK-015 have fractures visible in hand sample. The sample had an initial Leeb value similar to crystalline impactites (Table 7-8). This sample lost strength during weathering experiment (Fig 8). The sample also lost strength after desalination (Fig 8). The sample exhibits a slight gain in weight due to salt uptake during weathering experiment (Fig 9). After desalination, the sample lost more weight than after weathering experiment (Fig 9).

WCIS-14 MK-087 had initial Leeb value lower than crystalline rocks (Table 7-8). This sample lost very little strength during weathering experiment (Fig 8). The sample lost strength after desalination (Fig 8). The sample lost weight during weathering experiment and lost slightly more weight after desalination (Fig 9). The slight differences in the behaviour of both samples could be due to internal variation (e.g. macro-fractures, crystallites arrangement).

WCIS-14 MK-082 had initial Leeb value lower than crystalline impactites (Table 7-8). The sample lost strength due to the weathering experiment (Fig 8). The sample lost even more strength after desalination (Fig 8). The sample gained weight during weathering experiment possibly due to salt uptake (Fig 9). The sample lost a little weight after desalination (Fig 9).

WCIS-14 MK-082 exhibited the highest rate of deterioration among clast poor impact melt rocks.

3.2.3.3. Clast free impact melt rock

WCIS-14 MK-060 and WCIS-14 MK-077 are clast free impact melt rock. The sample had an initial Leeb value similar to crystalline rocks (Table 7-8). The samples lost strength during weathering experiment and after desalination (Fig 8). These samples lost a little weight during weathering experiment (Fig 9). The sample WCIS-14 MK-077 lost less weight during the weathering and desalination experiment than WCIS-14 MK-060 (Fig 9).

3.2.3.4. Lithic breccia

WCIS-14 MK-058B and WCIS-14 058C are lithic breccia which contains no melt. These samples had an initial Leeb value lower than crystalline impactites (Table 7-8). WCIS-14 058C has lower initial Leeb values compared to WCIS-14 MK-058B (Table 8). WCIS-14 MK-058B lost more strength during weathering and desalination experiment in comparison to WCIS-14 058C (Fig 8). WCIS-14 MK-058B showed more loss in weight than WCIS-14 058C after weathering experiment (Fig 9). After desalination WCIS-14 058C lost more weight than WCIS-14 MK-058B (Fig 9).

3.2.3.5. Impact melt-bearing breccia or suevite

Suevite (I), Suevite (II), and WCIS-14 Oz-005 are impact melt-bearing breccia or suevitic breccia. These samples had an initial Leeb value lower than crystalline impactites and similar to sedimentary impactites (Table 5-8). Suevite (II) contains more visible fracture and vitric clasts than Suevite (I). Suevite (II) and WCIS-14 Oz-005 lost strength during weathering experiment, but Suevite (I) gained strength (Fig 8). After desalination experiment, all samples lost strength, but Suevite (I) show a little loss in strength (Fig 8). Suevite (I) and Suevite (II) gained weight due to salt uptake during weathering experiment due to salt uptake through the macro-fractures (Fig 9). However, WCIS-14 Oz-005 lost weight during weathering experiment (Fig 9). After desalination, all the samples lost weight (Fig 9).

X-ray CT examination did not show any new fracture growth or change in existing fracture aperture and length due to weathering experiment in any of the samples.

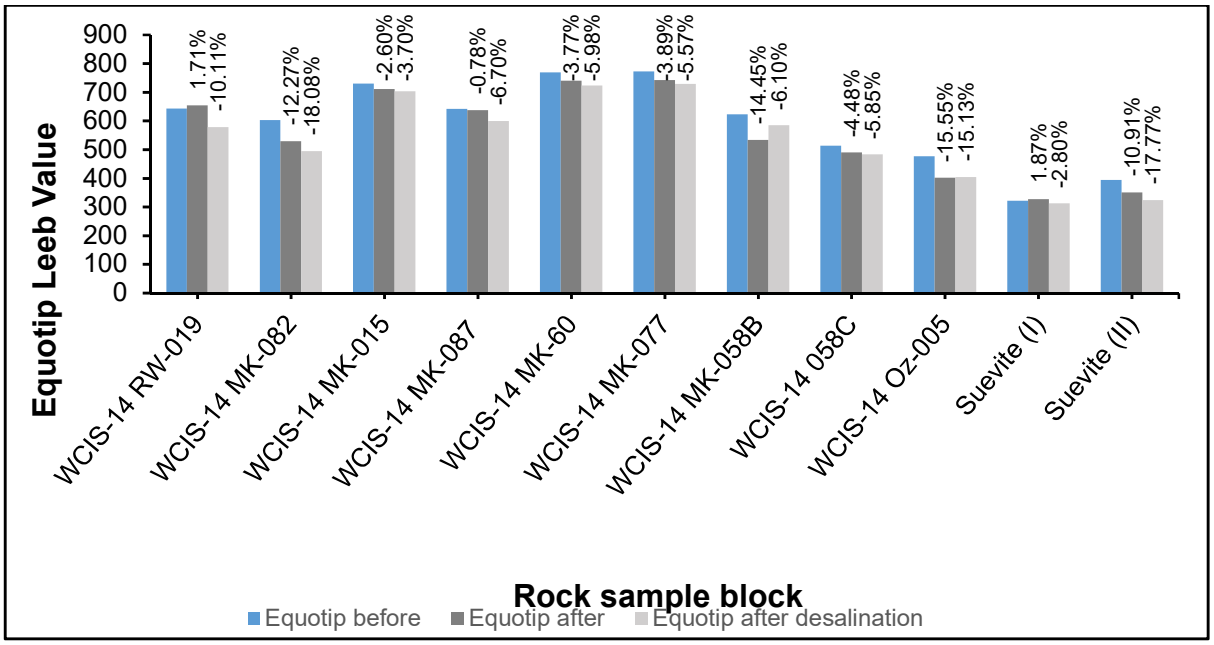

Fig 8. Change in Equotip Leeb Hardness value in Impact melt rock and impact breccia samples due to the weathering and desalination experiment. The percent value on top of each column is the percent change from initial leeb value.

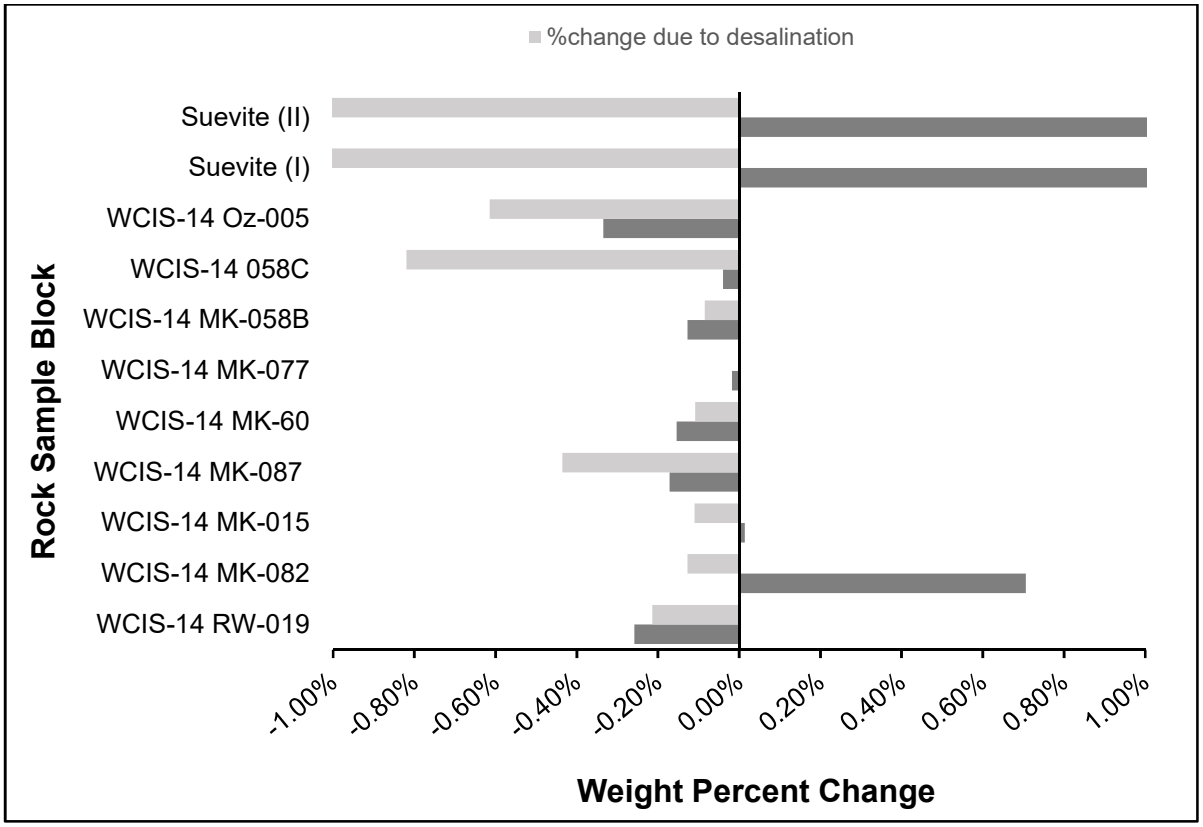

Fig 9. Percent weight change in impact melt rock and impact breccia samples due to the weathering and desalination experiment.

4. Discussion and interpretation

4.1. Role of simulated semi-arid environmental conditions

The decline in strength and loss of weight of the sample blocks under semi-arid terrestrial environment conditions demonstrates that the semi-arid environmental conditions may be sufficient to instigate breakdown. These findings suggest that relatively moderate rates of heating and cooling (dT/dt = ~0.15°C/min in this experiment) in the presence of salt and moisture can induce breakdown in rocks and the often cited 2°C/min thermal shock threshold is not required. Under the semi-arid conditions simulated in this study our experiment shows that rocks with impact inheritance tend to deteriorate faster than non-impacted rocks.

At night-time, cold conditions (low temperatures, lamp off) in the presence of high relative humidity, gypsum may have been mobilised. Lower loss or increase in strength in some impactites with macro-fractures compared to their counterparts with no visible macro-fractures or non-impacted control samples are noted due to the uptake of salt by the capillary rise through

fractures present in the bottom surface in contact with sand-salt layer. Because of its low mobility and solubility compared to other salts (e.g. sodium sulphate, sodium nitrate), gypsum tends to accumulate in the larger macro fracture opening (Charola et al., 2007), the accumulation of salt start to close the macro-fractures openings and inhibits subsequent ingress of salt and moisture (Smith et al., 2011). Similar behaviour was also recorded during initial cycles in laboratory weathering experiments for gypsum treated sandstone blocks by (Williams and Robinson, 2001) and other sodium sulphate treated sandstone (Ghobadi and Babazadeh, 2015) and crystalline rocks (Viles et al., 2010; Viles et al., 2018; Zhu et al., 2003). However, after removal of salts by desalination experiment, these samples exhibited a loss in strength. This suggests that if the length of our experiment were longer, the weakening of blocks that have taken up salt would have occurred. The effectiveness of salt depends on a combination of its solubility, rate of solubility changes with temperature, crystal habit, the rate of crystal growth and volume increases associated with hydration/dehydration changes (Warke, 2007). Due to its low solubility and mobility, gypsum salts are not as aggressive as other more soluble salts such as sodium sulphate and sodium nitrates. However, in the presence of other salt species and more extended exposure in the environment gypsum salts can cause a breakdown in rocks as the initial cementing role of salts is replaced by a deteriorative role (Charola et al., 2007; Williams and Robinson, 2001).

4.2. Size and shape of the blocks

Some of the sample blocks used in the weathering experiment were cuboidal instead of a cube, and few of them had a smaller dimension ca. 3 cm. In order to understand the possible effects of variations in size and shape of blocks on weathering experiment results, we tested blocks with slight variation in size and shape. We obtained blocks of different size and shape (cube and cuboid in this experiment) from a few larger samples collected in the field. In the experiment, we found that a small (~ 1-2 cm in side length) variation in size and shape did not affect the response of sample blocks due to the weathering experiment. The block response is more influenced by internal variation (e.g. presence and distribution of flaws such as fractures and laminations, distribution of vitric phases in the sample) than the size and shape of the blocks.

4.3. Severity and mode of deterioration

Our weathering experiment simulated natural semi-arid field conditions for a short duration of time. This did not have a significant effect on most of the blocks, and no severe damage was observed compared to those observed in a longer weathering experiment simulations (e.g. (Warke, 2007)

Small amounts (0.03 g) of granular disintegration was noticed in some of the Class 1a MS samples (Fig 10), and class 1b CS sample. A few of the impact melt rocks (WCIS-14 MK-082), and impact melt-bearing breccias (Suevite I and Suevite II) also lost material due to granular disintegration. Class 1a Coconino Sandstone lost measurable mass through granular disintegration, but due to the similar colour of the base sand layer, it was difficult to differentiate between the debris and sand used in the experiment.

We also observed salt efflorescence on many sample blocks in contact with the sand-salt layer in the experiment.

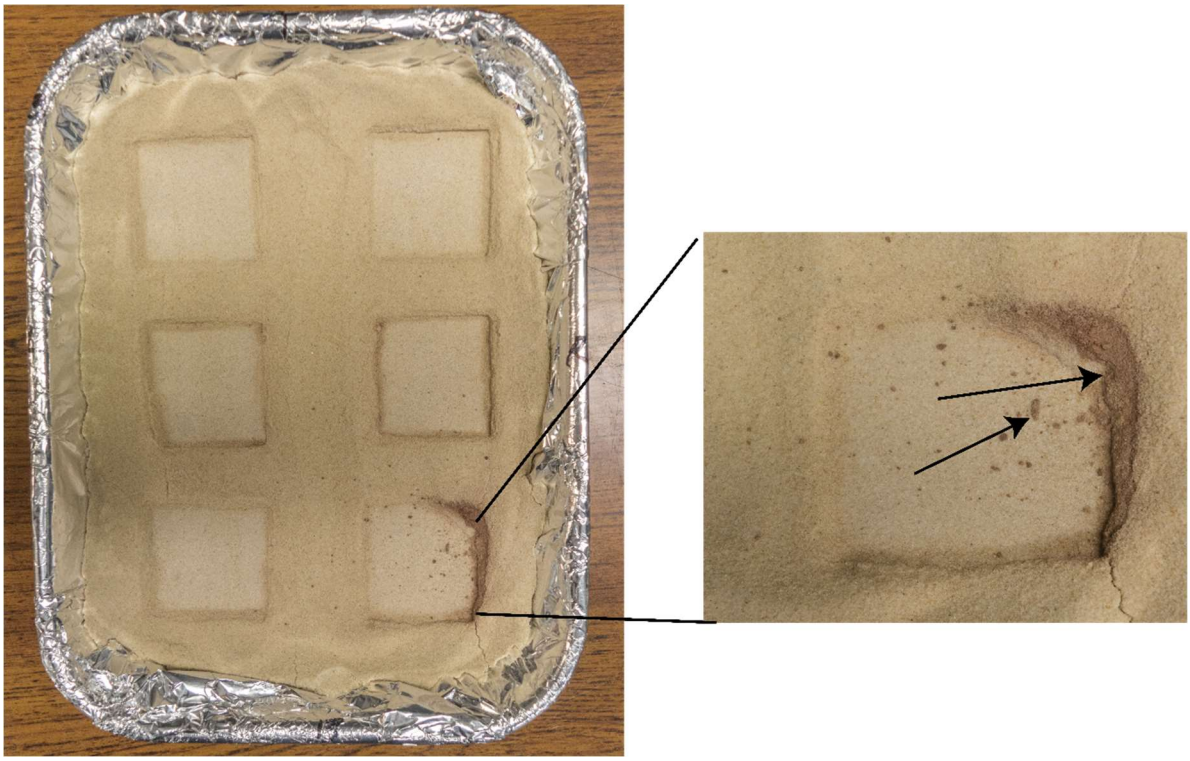

Fig 10. The observed breakdown in rock samples. Black arrows show chips and granular disintegrated material in class 1a MS after the sample block is removed from the bed.

4.4. Fracture propagation

The sample blocks were monitored using X-ray CT before and after the weathering experiment to understand the role of impact generated macroscopic fractures to subsequent weathering. CT scans were helpful in visualising and quantifying pre-existing fractures in the blocks (Fig 11). While no changes in aperture or length of the fractures were observed following the weathering experiment in CT images, some factors may be responsible for this. First, the resolution of CT images (46 μm) may not have been sufficient to resolve any changes in existing fractures or indeed detect a newly generated fracture. Second, the weathering simulation may not have produced any change. Regardless, we are confident that this technology, which can yield higher resolutions, will enable a better understanding of rock response that is normally not accessible to the investigator to assess a change in the short length.

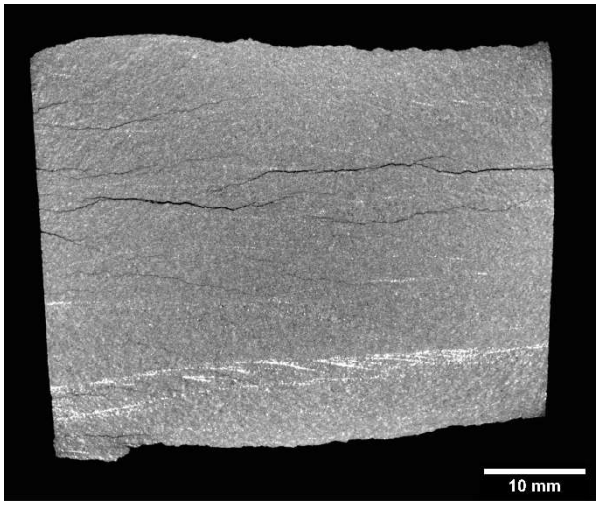

Fig 11. Macro-fractures seen in a class 1a MS (MC51317-4_I) block in X-ray CT image. The aperture of fractures ranges from 0.09-0.2 mm. In the bottom portion of the sample, one set of cross laminations is visible. Resolution of the image is 46 μm/voxel.

4.5. Lithology

In our experiment, different impactites were subjected to identical weathering conditions. Thus the results can be broadly compared.

There was no significant difference in initial strength of class 1a shocked and unshocked control CS samples. Even though porosity is reduced in class 1a CS compared to unshocked CS (Table 1), class 1a CS showed an accelerated loss of strength in comparison with unshocked CS. This may be due to the presence of irregular intragranular fractures in quartz grains. It is likely that intragranular fractures are exploited and enlarged by thermal stressing in the

presence of salt and moisture. This would lead to an accelerated weakening in class 1a Coconino Sandstone. In previous studies, it was noted that the CS samples are also weaker along lamination planes (Kieffer, 1971a). The passage of shock wave in the Coconino Sandstone may also have made samples weaker along these laminations (Kieffer, 1975).

At shock pressure class 1b, the passage of shock wave has caused weak lithification in CS due to extensive grain fracturing and comminution (Kieffer, 1975). As a result, the CS has become friable and easily breaks down under slight hand pressure. This sample had lower initial strength compared to class 1a and unshocked CS, as the sample was so soft that equotip measurement was not possible. Primary porosity was reduced in this sample due to compaction and grain rotation. However, similar to sample 1a, secondary porosity due to grain fracturing support the ingress of salt and moisture. The sample easily loses mass due to granular disintegration. This sample showed evidence of more rapid breakdown relative to all other samples. Suggesting, that even in low shocked rocks of specific lithologies, an increase in shock influences breakdown rates, if not styles of breakdown. Future access to samples for experimental work will permit these findings to be validated.

Although not statistically significant, we found that the trend is for weathering of Coconino Sandstone to have been more strongly expressed relative to Moenkopi Sandstone in the low shock pressure deformation class (1a). This can be due to two reasons –

1. Coconino Formation being the closest to the point of impact might have experienced relatively higher shock deformation in low shock pressure regime (0-5 GPa) compared to Moenkopi Formation which represents the free surface of the impact site (Kring, 2017).
2. The finer grain size of Moenkopi Sandstone (0.07-0.1 mm) and low porosity (5-8%) when compared to Coconino Sandstone (grain size = 0.09-0.16 mm, porosity = 20%), may have led to a different response in low shock pressure regime (0-5 GPa). Class 1a MS only exhibits a reduction in porosity, unlike class 1a CS, it is not affected by irregular fracturing in quartz grains. This difference may be key in the subsequent expression of rock breakdown in sandstone.

The response of specific samples during the experiments did not always indicate the final outcome. We found a significant difference in the response of the class 1a MS which initially showed a decrease in strength but at the end of the cycle, showed a trend to increase in strength,

although, not back to initial values. Unshocked Moenkopi Sandstone did not have this trend. We hypothesise that this is due to the higher frequency of macro-fractures in the class 1a MS that creates accommodation space for the precipitation of salts. Class 1a MS that had macrofractures became stronger due to the ingress of salts via macrofractures. However, following de-salination the rock samples exhibited an accelerated decrease in strength compared to unshocked and other class 1a MS. This suggests that macro-fractures in class 1a MS samples are compensating for the loss in porosity and if the experiment were extended in duration, perhaps class 1a samples may have shown higher deterioration relative to unshocked samples.

Unusually class 1a CS gained strength following desalination. This may be due to grain size, composition and packing difference in two different types of sandstone (Israeli and Emmanuel, 2018). However, there is no conclusive explanation for this behaviour of class 1a CS since this was not observed in unshocked CS.

Class 1a crystalline granite and tonalite were much stronger than Coconino and Moenkopi Sandstone. These rocks have coarser grains and smaller macro-fractures than MS samples. These samples had a negligible primary porosity (0.07-0.2 %), however intergranular(?) and intragranular fracturing in these rocks created space for moisture and salt ingress. The smaller pores in crystalline impactites limited the initial salt and moisture penetration whereas macro-fractures aided in ingress of salt and moisture. After a few wetting cycles, cementation of salt in macro-fractures blocked the subsequent ingress of moisture and salt in the fracture openings. These rocks showed a muted response during weathering experiment. After removal of cemented salts by desalination experiment the rocks show a higher loss of strength. This loss of strength was comparable to low shocked sandstone samples. Nevertheless, low shocked crystalline impactites do not lose material as much as low shocked sedimentary impactites due to weathering and desalination experiment because these samples are much stronger than sandstone samples and require longer stressing to start deterioration.

Impact melt-bearing breccias or suevites were weaker than crystalline rocks, lithic breccias and impact melt rocks but have similar strength as class 1a sandstone. Impact melt-bearing breccia exhibited the highest loss in strength and weight among impact breccias and impact melt rocks. They deteriorate faster than class 1a sandstone and crystalline rocks.

Lithic breccias are weaker than crystalline rocks and impact melt rocks but were as strong as class 1a sandstone. The loss of strength in lithic breccias was higher than impact melt rocks but similar to class 1a sandstone and crystalline rocks.

Heterogeneous and anisotropic nature of gains and lithic fragment arrangement by finer grained matrix made impact melt breccia and lithic breccia less cohesive than other impactites. The coefficient of thermal expansion and heat capacity of different crystalline and amorphous phases are different (Fei, 1995; Navrotsky, 1995). Mismatch in the thermal response of neighbouring grains due to these thermal properties may enhance deterioration due to heating and cooling. Because of the heterogeneous arrangement of grains, impact breccias might experience higher thermal fatigue due to thermal cycling.

Impact melt rocks are weaker than crystalline rocks but are stronger than impact melt-bearing breccia, lithic breccia and class 1a sandstone. The impact melt rocks with increasing clast density showed higher loss in strength. The clast free impact melt rock showed lower loss in strength compared clast rich and clast poor impact melt rocks due to weathering and desalination experiment. One clast poor fine-grained impact melt rock (WCIS-14 MK-082) exhibited the highest loss in strength due to weathering and desalination experiment among all the samples. This sample had lower strength than other impact melt rocks (Table 8). This sample was stronger than impact melt-bearing breccia and sandstone but weaker than crystalline rocks. The accelerated loss in strength in this sample may because it was more chemically altered than other impact melt rocks.

In this experiment, we found that class 1b Cononino Sandstone will breakdown the fastest followed by impact melt-bearing breccias, altered impact melt rock, lithic breccia, class 1a Coconino Sandstone, class 1a Moenkopi Sandstone, impact melt rock, and class 1a crystalline rock (Fig 12). This order of breakdown is proposed based on the observation of deterioration and initial strength of the samples used in this experiment.

Fig 12. Relative rates of breakdown observed on sample rocks following experiments. Highest rates are at the bottom. 'T' represents the top surface of the sample block.

4.6. The implication for rock breakdown on Early Mars

During the early history of Earth and Mars, the rate of impact was very high (Wetherill, 1975). More than 350,000 impact craters with a diameter ≥1 km have been documented on Mars (Robbins and Hynek, 2012). Impactites are expected to be present in craters on Mars. Osinski and Melosh (2004) suggested that a diverse range of impactites should also be expected on Mars, given the role of volatiles in the generation and deposition of ejecta (Weiss and Head, 2014). During the last two decades, unmanned missions roving the surface of Mars as well as orbiters have confirmed the detection of impactites such as impact breccia (Hayes et al., 2011), lithic impact breccia (Squyres et al., 2012), impact melt breccia (Arvidson et al., 2014; Squyres et al., 2012), impact spherules and tektites (Kah, 2015; Newsom et al., 2014), impact melts and glasses (Schultz and Mustard, 2004) as well as fractured target rocks.

A question currently under discussion for Mars is whether the aqueous alteration processes occurred episodically or were sustained over periods sufficiently long to sustain habitable environment on Mars (Des Marais et al., 2008). Understanding the nature and rate of weathering can help answer this question and constrain the past climate on Mars and perhaps contribute to the early "warm and wet" (Carter et al., 2015) versus "cold and icy" (Fairén, 2010) climate debate (Ming et al., 2008; Palumbo and Head, 2017). Viles et al. (2010) ran Mars weathering simulations for 12 days on basalt and found that rocks with stress history will deteriorate due to thermal cycling in present-day Mars conditions. They report no change in rock strength for rocks that were not pre-stressed. Even though regolith and rocks on Mars have different mineralogy than rocks used in our experiment, the results of this work have implications for Martian rock breakdown. The shock effects will produce broadly similar deformations and heterogeneities in the rocks that will affect the subsequent weathering of rocks.

During the Noachian period (approx. 4100 to 3700 million years ago), Mars possessed an atmosphere about as dense as Earth's, but most of it was lost to space due to solar wind and ultraviolet rays. The early climate of Mars was suitable to support chemical weathering (Zolotov and Mironenko, 2016). Noachian craters are widespread on Mars. Cratering events during Noachian would have produced an enormous amount of impactites consisting of shocked crystalline minerals and impact glasses (Boslough, 1991; Schultz and Mustard, 2004). It is known from laboratory experiments that shocked mafic, and impact glasses dissolves faster than the unshocked crystalline counterparts (Bell, 2015; Bell, 2017; Boslough and Cygan,

1988; Cygan et al., 1989). These shock activated minerals require less time to alter and intermittent warming events due to impact, and volcanic events might be enough to weather these minerals (Halevy and Head III, 2014; Palumbo and Head, 2018). Most of the altered material dates from the Noachian and Early Hesperian (Poulet et al., 2005; Tornabene et al., 2013), period of heaviest meteorite bombardment, so these materials have continued to be exposed for subsequent shock modification and shock activated weathering process occurring in synergy for billions of years (Boslough, 1991; Tyburczy and Aherns, 1988). These two processes in combination may be responsible for abundant dust and colour of Martian fines on Mars (Boslough, 1991; Boslough et al., 1986).

Our understanding of impact-induced modification and activation processes on subsequent weathering is limited on Mars. Most of the cratering of terrestrial and Martian surface occurred during the period of early bombardment in the solar system, and therefore, these rocks have been exposed for billions of years to the weathering environment on Mars. Several studies have reported that most of the hydrous alteration minerals (i.e. phyllosilicates) on Mars are associated with impact craters and old cratered terrain (Carter et al., 2015; Ehlmann and Edwards, 2014; Loizeau et al., 2015; Tornabene et al., 2013). This suggests that the crater landforms housed lacustrine environments, where enhanced hydrological processes would have been in operation. These impact shock processes and the impact gardening of surface material on Mars have been the dominant process that contributed to the evolution of chemical, mineralogical, and physical properties of the Martian regolith (Boslough, 1991; Knauth et al., 2005)

During Noachian and Hesperian periods, when the Martian climate was different from today, and it is intuitive to suggest that fluids were available to react with rocks (Carter et al., 2015; Zolotov and Mironenko, 2016). To date, inheritance has not been considered in the discussion of surface features on Mars, particularly the inheritance of weakness in rocks due to impact. The results of the experimental work suggest that impactites would have broken down faster than non-impact rocks. It is also likely; this would have been expressed along a shock magnitude continuum (although this has yet to be demonstrated). This latter point is supported somewhat by the work of other researchers to understand shock enhanced weathering of mafic and plagioclase minerals. They found that the rate of dissolution of minerals is controlled by the shock level, and shocked minerals alter faster than the unshocked minerals (Bell, 2017; Boslough and Cygan, 1988). In addition, it has been found that the significant volume of impact glasses formed during impact would react faster than their crystalline counterparts (Cannon

and Mustard, 2015; Tornabene et al., 2013; Wolff-Boenisch et al., 2006). Enhanced weathering of impactites in Noachian cratered terrain may be the reason for the abundance of hydrated silicates and clay minerals in these regions (Poulet et al., 2005). Even under less hydrous scenarios for an early Mars, the impact-induced fracture planes at the mineral and clast scale would have been important controls to induce rapid breakdown under 'cold-icy' thermal cycles.

Sedimentary rocks on Mars are more common than previously thought: with the advancement in remote sensing data collection during the last 20 years, sedimentary rocks have been identified at various locations on that planet (Malin and Edgett, 2000). However, these rocks have a mafic to ultramafic composition and are different in mineralogy than commonly found sedimentary rocks on Earth (McLennan and Grotzinger, 2008). Meridiani Planum has several impact craters in sedimentary target rocks (e.g. Victoria Crater; (Hayes et al., 2011; Squyres et al., 2009). As different rock types experience a different level of shock damage depending on porosity, mineralogy, volatile saturation, and distance from the point of impact during impact (Kieffer, 1971a), sedimentary rocks can be more affected compared to crystalline rocks experiencing the same shock pressure level. Even a low shock pressure (<10 GPa) causes more damage in sedimentary rocks (e.g. sandstone; (Kieffer, 1971b) than in crystalline rocks (e.g. basalt; (Kieffer et al., 1976a). This study supports this finding where we find that sandstone that has experienced the same level of low shock pressure will breakdown faster than crystalline rocks.

The difference in rock types and facies may produce a difference in impact shock-related damage, and this will subsequently lead to a differential rate of rock breakdown. This suggests that the erosion/degradation of crater landforms will differ depending on the lithology of the target rock. Regional and local differences in lithology may lead to a differential rate of breakdown. Weak lithification caused due to low impact shock would produce weak rock materials that could be easily removed by fluvial and aeolian erosional processes (Grant et al., 2008; Kieffer, 1975). For example, Class 1b Coconino Sandstone has become so soft and friable that it can be easily removed in the field by aeolian or fluvial processes. Similar aeolian erosion of weaker sandstone (aeolianite) rocks are also reported at Victoria Crater on Mars (Grant et al., 2008). Despite the discovery of several hundreds of potential paleolakes, relatively rarity of the preserved delta deposits on Mars is a mystery (Fassett and Head III, 2008; Hoke et al., 2014; Howard, 2007). This sparse presence of delta deposits may be explained by resurfacing by a combination of impact processes and aeolian erosion. Impact

processes produce weaker and friable impacted rock material that is subsequently removed by aeolian processes and limit their preservation.

The age of the Martian surface is determined by crater count statistics (Hartmann and Neukum, 2001). The crater chronology models are based on crater size-frequency distribution on the surface of Moon, which is linked to the radiometric age of lunar samples and meteorites (Hartmann and Neukum, 2001; Werner and Tanaka, 2011). Enhanced weathering and erosion of shocked ejecta and impactites in different lithologies may affect the preservation of crater diameters or indeed may control the enhanced modification of crater rims. These factors have not received sufficient attention in the literature.

Regolith on the lunar surface consists of minerals shocked at various levels and impact glass (Kieffer, 1975), but The Moon lacks an atmosphere or hydrosphere with which the regolith can react. On airless bodies, thermal gradients are considerably high compared to planetary bodies with the atmosphere (Molaro and Byrne, 2012). Impact-induced deformation and discontinuities will subsequently affect the thermal breakdown of rocks and production of regolith on asteroids and planetary bodies without an atmosphere (Delbo, 2014; Hazeli et al., 2017; Viles, 2014).

5. Conclusion

This study is the first systematic attempt to understand the effect of impact generated heterogeneities and deformation on the subsequent weathering of impactites. A physical weathering experiment on impactites was conducted for the first time in an environmental chamber. Several types of impactites were subjected to physical weathering experiment in simulated terrestrial semi-arid environmental conditions. These impactites include low shocked Coconino and Moenkopi Sandstone from Meteor Crater, low shocked Granite and Tonalite, impact melt rocks, lithic breccias, and impact melt-bearing breccia from West Clearwater Impact Structure, and Suevite breccia from Ries Crater.

The major results summarised as follows.

1. Low shock pressure (<5 GPa) causes pore collapse and macro- and micro-fracturing in porous sandstone. The macro- and micro-fractures make sandstone weaker and guide the entry of moisture and salt and so have a control on the intensity of weathering. Low

shocked (class 1a and 1b) sandstone exhibits accelerated deterioration than unshocked counterparts.

2. Low shocked crystalline impactites (<10GPa) exhibit similar loss of strength comparable to low shocked sandstone samples. Nevertheless, low shocked crystalline impactites were stronger than low shocked sedimentary impactites. They do not lose material as much as low shocked sedimentary impactites due to weathering and desalination experiment as these samples will require longer stressing to start deterioration.
3. Impact melt bearing breccia were weaker and less cohesive compared to impact melt rocks, lithic breccia and class 1a crystalline and sedimentary impactites. These samples breakdown faster than other samples.
4. Lithic breccias have strength comparable to low shocked sedimentary impactites. The rate of deterioration of these samples are similar to low shocked sedimentary impactites.
5. The impact melt rocks have strength comparable to low shocked crystalline impactites. The impact melt rocks with increasing clast density show accelerated loss in strength. This is because as the clast content decreases, welding action of melt becomes stronger. For example, Clast free impact melt rocks are stronger than clast rich impact melt rocks.
6. Since melt and glasses are more susceptible to chemical alteration than their crystalline counterparts (Wolff-Boenisch et al., 2006). Once the impact melt rocks are chemically altered, their breakdown is faster than low shocked sedimentary and crystalline impactites due to subsequent physical weathering (e.g. WCIS-14 MK-082 in our experiment).
7. Our weathering experiment successfully simulated realistic spring-time semi-arid temperature regimes and demonstrated that the semi-arid environmental conditions might be sufficient to instigate breakdown. Relatively moderate rates of heating and cooling (dT/dt = ~0.15°C/min in this experiment) in the presence of salt and moisture can induce breakdown in rocks and often-cited 2°C/min thermal shock threshold may not be necessary.
8. A small variation in clast shape and size does not significantly affect the response of sample blocks in the weathering experiment. The response of the blocks is more affected by internal variation (e.g. presence and distribution of flaws such as fractures and laminations, distribution of vitric phases in the sample).
9. Granular disintegration and salt efflorescence are two of the observed breakdown features in the sample blocks after the weathering experiment. X-ray CT examination

of samples at a resolution of 46 µm revealed no change in existing macro-fractures and no new fractures. The changes in macro-fractures may occur below the detection limit of 46 µm.

We found that impactites exhibited an accelerated decline in strength compared to non-impacted control samples. However, the rock type and impact deformation history are important in controlling the rate of deterioration. As impact craters are widespread on Mars, the enhanced breakdown of impactites are likely to have played an important role in landscape evolution on Mars. Even on airless bodies, the impact generated discontinuities and heterogeneities can be exploited by thermal cycling to produce an accelerated breakdown (Hazeli et al., 2017).

Acknowledgements

The authors would like to thank Dr David Kring and Dr Niamh Cullen for their assistance in collecting samples at Meteor Crater and the control sites. The Prosser family, Meteor Crater Enterprises, and Barringer family kindly allowed the authors to access the Bar T Bar Ranch property near Meteor Crater in Arizona for collecting Moenkopi and Coconino Sandstone samples. A myriad thanks must go to Dr Farah Ahmed, Dr Jens Najorka, Dr Amin Garbout, and Dr Tobias Salge for hosting AKV at Natural History Museum in London and training him to collect data using X-ray diffraction and X-ray computed tomography (CT). Dr Robbie Goodhue, Mr Neil Kearny and Mr Noel McGinley are thanked for their help in Geology labs at Trinity College Dublin. Mr Frances Hendron is thanked for preparing thinsections and cutting rock samples. Mr Colin Reid, Ms Leona O'Connor, Dr Paul Guyett are thanked for their help using Scanning Electron Microscope at Centre for Microscopy and Analysis. A big thanks Dr James Canavan at the Geography department for their assistance in preparations for lab work. All the technical staff at Oxford Rock Breakdown Laboratory - Dr Mona Edwards, Dr Hong Zhang, and Mr Ayush Srivastava are thanked for their warm hospitality and help in conducting the Physical weathering experiment. Ankit K. Verma was supported by the following: Trinity College Dublin Postgraduate Studentship, Faculty of Engineering, Maths and Science, Trinity College Dublin, India (PhD) Scholarship, the J.N. Tata Endowment Scholarship for the higher education of Indians, and the J.N. Tata Gift Scholarship during the preparation of this paper; The Barringer Family Fund for Meteorite Impact Research 2015, British Society for Geomorphology Postgraduate Research Grant 2016, International

Association of Sedimentologists Postgraduate Research Grant 2016, Trinity Association and Trust Travel Grant and Trinity Trust Travel Grant 2016 for field work; Europlanet 2020 Research Infrastructure Access Grant (Europlanet 2020 RI has received funding from the European Union's Horizon 2020 research and innovation programme under grant agreement No 654208) for lab work at Natural History Museum, London.

References

Anders, M. H., Laubach, S. E., Scholz, C. H., 2014. Microfractures: A review. Journal of Structural Geology. 69**,** 377-394.

Aoki, H., Matsukura, Y., 2007. A new technique for non-destructive field measurement of rock-surface strength: an application of the Equotip hardness tester to weathering studies. Earth surface processes and landforms. 32**,** 1759-1769.

Arvidson, R., et al., 2014. Ancient aqueous environments at Endeavour crater, Mars. Science. 343**,** 1248097.

Bell, M., 2015. Experimentally Shocked and Altered Basalt: Laboratory Analogs for Calibration of Mars Remote Sensing and In Situ Data.

Bell, M., 2017. Experimentally Shocked and Altered Basalt: VNIR Spectra of Mars Analog Materials.

Boslough, M., 1991. Shock modification and chemistry and planetary geologic processes. Annual Review of Earth and Planetary Sciences. 19**,** 101-130.

Boslough, M., Venturini, E., Morosin, B., Graham, R., Williamson, D., 1986. Physical properties of shocked and thermally altered nontronite: Implications for the Martian surface. Journal of Geophysical Research: Solid Earth. 91.

Boslough, M. B., Cygan, R. T., 1988. Shock-enhanced dissolution of silicate minerals and chemical weathering on planetary surfaces. Lunar and Planetary Science Conference Proceedings, Vol. 18, pp. 443-453.

Bruker, A., Topas, V. J. B., Karlsruhe, 2003. 1: general profile and structure analysis software for powder diffraction data–User manual.

Buckman, J., Bankole, S. A., Zihms, S., Lewis, H., Couples, G., Corbett, P. W., 2017. Quantifying Porosity through Automated Image Collection and Batch Image Processing: Case Study of Three Carbonates and an Aragonite Cemented Sandstone. Geosciences. 7**,** 70.

Buhl, E., Poelchau, M. H., Dresen, G., Kenkmann, T., 2013. Deformation of dry and wet sandstone targets during hypervelocity impact experiments, as revealed from the MEMIN Program. Meteoritics & Planetary Science. 48**,** 71-86.

Buscombe, D., 2013. Transferable wavelet method for grain-size distribution from images of sediment surfaces and thin sections, and other natural granular patterns. Sedimentology. 60**,** 1709-1732.

Cannon, K. M., Mustard, J. F., 2015. Preserved glass-rich impactites on Mars. Geology. 43**,** 635-638.

Carter, J., Loizeau, D., Mangold, N., Poulet, F., Bibring, J.-P., 2015. Widespread surface weathering on early Mars: A case for a warmer and wetter climate. Icarus. 248**,** 373-382.

Charola, A. E., Pühringer, J., Steiger, M., 2007. Gypsum: a review of its role in the deterioration of building materials. Environmental geology. 52**,** 339-352.

Cockell, C. S., Osinski, G. R., 2007. Impact-induced impoverishment and transformation of a sandstone habitat for lithophytic microorganisms. Meteoritics & Planetary Science. 42**,** 1985-1993.

Cygan, R. T., Casey, W. H., Boslough, M. B., Westrich, H. R., Carr, M. J., Holdren, G. R., 1989. Dissolution kinetics of experimentally shocked silicate minerals. Chemical geology. 78**,** 229-244.

De Kock, T., et al., 2015. A pore-scale study of fracture dynamics in rock using X-ray micro-CT under ambient freeze–thaw cycling. Environmental science & technology. 49**,** 2867-2874.

Delbo, M., 2014. Thermal fatigue as the origin of regolith on small asteroids. Nature. 508**,** 233-236.

Des Marais, D., Jakosky, B. M., Hynek, B. M., 2008. Astrobiological implications of Mars' surface composition and properties. The Martian Surface-Composition, Mineralogy, and Physical Properties. 1**,** 599.

Ehlmann, B. L., Edwards, C. S., 2014. Mineralogy of the Martian surface. Annual Review of Earth and Planetary Sciences. 42**,** 291-315.

Engelhardt, W., 1997. Suevite breccia of the Ries impact crater, Germany: Petrography, chemistry and shock metamorphism of crystalline rock clasts. Meteoritics & Planetary Science. 32**,** 545-554.

Fairén, A. G., 2010. A cold and wet Mars. Icarus. 208**,** 165-175.

Farquharson, J., Griffiths, L., Baud, P., Wadsworth, F., Heap, M., 2017. Compressive strength evolution of thermally-stressed Saint Maximin limestone. AGU Fall Meeting Abstracts.

Fassett, C. I., Head III, J. W. J. I., 2008. Valley network-fed, open-basin lakes on Mars: Distribution and implications for Noachian surface and subsurface hydrology. 198**,** 37-56.

Fei, Y., 1995. Thermal expansion. Mineral physics & crystallography: a handbook of physical constants. 2**,** 29-44.

Ferrière, L., Osinski, G. R., 2013 Shock metamorphism. In: G. R. Osinski, E. Pierazzo, (Eds.), Impact cratering: Processes and products. John Wiley & Sons, pp. 106-124.

French, B. M., Koeberl, C., 2010. The convincing identification of terrestrial meteorite impact structures: What works, what doesn't, and why. Earth-Science Reviews. 98**,** 123-170.

Furukawa, Y., Sekine, T., Kakegawa, T., Nakazawa, H., 2011. Impact-induced phyllosilicate formation from olivine and water. Geochimica et Cosmochimica Acta. 75**,** 6461-6472.

Ghobadi, M., Babazadeh, R., 2015. Experimental studies on the effects of cyclic freezing–thawing, salt crystallization, and thermal shock on the physical and mechanical characteristics of selected sandstones. Rock Mechanics and Rock Engineering. 48**,** 1001-1016.

Goudie, A., Parker, A., 1998. Experimental simulation of rapid rock block disintegration by sodium chloride in a foggy coastal desert. Journal of Arid Environments. 40**,** 347-355.

Goudie, A. S., Wright, E., Viles, H. A., 2002. The roles of salt (sodium nitrate) and fog in weathering: a laboratory simulation of conditions in the northern Atacama Desert, Chile. Catena. 48**,** 255-266.

Grant, J. A., et al., 2008. Degradation of Victoria crater, Mars. Journal of Geophysical Research: Planets. 113.

Grieve, R. A., Therriault, A. M., 2013. Impactites: Their characteristics and spatial distribution. Impact cratering: Processes and products. 90-105.

Halevy, I., Head III, J. W., 2014. Episodic warming of early Mars by punctuated volcanism. Nature Geoscience. 7**,** 865.

Hartmann, W. K., Neukum, G., 2001 Cratering chronology and the evolution of Mars. Chronology and evolution of Mars. Springer, pp. 165-194.

Hayes, A., Grotzinger, J., Edgar, L., Squyres, S., Watters, W., Sohl-Dickstein, J., 2011. Reconstruction of eolian bed forms and paleocurrents from cross-bedded strata at Victoria Crater, Meridiani Planum, Mars. Journal of Geophysical Research: Planets. 116.

Hazeli, K., El Mir, C., Papanikolaou, S., Delbo, M., Ramesh, K., 2017. The Origins of Asteroidal Rock Disaggregation: Interplay of Thermal Fatigue and Microstructure. Icarus.

Hoke, M. R., Hynek, B. M., Di Achille, G., Hutton, E. W. J. I., 2014. The effects of sediment supply and concentrations on the formation timescale of Martian deltas. 228**,** 1-12.

Howard, A. D. J. G., 2007. Simulating the development of Martian highland landscapes through the interaction of impact cratering, fluvial erosion, and variable hydrologic forcing. 91**,** 332-363.

Israeli, Y., Emmanuel, S. J. E. S. D., 2018. Impact of grain size and rock composition on simulated rock weathering. 6**,** 319-327.

Kah, L. C., 2015. Images from Curiosity: A New Look at Mars. Elements. 11**,** 27-32.

Kenkmann, T., Poelchau, M. H., Wulf, G., 2014. Structural geology of impact craters. Journal of Structural Geology. 62**,** 156-182.

Kieffer, S., Schaal, R., Gibbons, R., Horz, R., Milton, D., Dube, A., 1976a. Shocked basalt from Lonar impact crater, India, and experimental analogues. Lunar and Planetary Science Conference Proceedings, Vol. 7, pp. 1391-1412.

Kieffer, S. W., 1971a. I. Shock metamorphism of the Coconino sandstone at Meteor Crater, Arizona. II. The specific heat of solids of geophysical interest. California Institute of Technology.

Kieffer, S. W., 1971b. Shock Metamorphism of the Coconino Sandstone. Journal of Geophysical Research.

Kieffer, S. W., 1975. From regolith to rock by shock. The Moon. 13**,** 301-320.

Kieffer, S. W., Phakey, P. P., Christie, J. M., 1976b. Shock processes in porous quartzite: Transmission electron microscope observations and theory. Contributions to Mineralogy and Petrology. 59**,** 41-93.

Knauth, L. P., Burt, D. M., Wohletz, K. H., 2005. Impact origin of sediments at the Opportunity landing site on Mars. Nature. 438**,** 1123-1128.

Kompatscher, M., 2004. Equotip-rebound hardness testing after D. Leeb. Proceedings, Conference on Hardness Measurements Theory and Application in Laboratories and Industries, pp. 11-12.

Kring, D. A., 2017. Guidebook to the geology of Barringer Meteorite Crater, Arizona (aka Meteor Crater): for the 80th Annual Meeting of the Meteoritical Society July 2017. Lunar and Planetary Institute.

Leroux, H., 2005. Weathering features in shocked quartz from the Ries impact crater, Germany. Meteoritics & Planetary Science. 40**,** 1347-1352.

Loizeau, D., et al., 2015. Widespread Surface Weathering on Early Mars: possible implication on the Past Climate. EGU General Assembly Conference Abstracts, Vol. 17.

Madden, M. E. E., Kring, D. A., Bodnar, R. J., 2006. Shock reequilibration of fluid inclusions in Coconino sandstone from Meteor Crater, Arizona. Earth and Planetary Science Letters. 241**,** 32-46.

Malin, M. C., Edgett, K. S., 2000. Sedimentary rocks of early Mars. Science. 290**,** 1927-1937.

McLennan, S., Grotzinger, J., 2008. The sedimentary rock cycle of Mars. The Martian Surface-Composition, Mineralogy, and Physical Properties. 1**,** 541.

Ming, D. W., Morris, R. V., Clark, B. C., 2008. Aqueous alteration on Mars. The Martian Surface—Composition, Mineralogy, and Physical Properties. 519.

Molaro, J., Byrne, S., 2012. Rates of temperature change of airless landscapes and implications for thermal stress weathering. Journal of Geophysical Research: Planets (1991–2012). 117.

Navrotsky, A., 1995. Thermodynamic properties of minerals. Mineral Physics & Crystallography: a handbook of physical constants. 18-28.

Newsom, H. E., et al., 2014. Gale crater and impact processes–Curiosity's first 364 Sols on Mars. Icarus.

Newsom, H. E., Wright, S. P., Misra, S., Hagerty, J. J., 2013. Comparison of simple impact craters: A case study of Meteor and Lonar Craters. Impact Cratering: Processes and Products. 271-289.

Osinski, G., Grieve, R., 2017. " Suevites" of the West Clearwater Lake Impact Structure, Canada: A Demonstration of the Need for a Revised Classification Scheme for Impactites. Lunar and Planetary Science Conference, Vol. 48.

Osinski, G., Melosh, H., 2004. Impactites on Mars: What Should We Expect and What is the Role of Volatiles? , Second Conference on Early Mars: Geologic, Hydrologic, and Climatic Evolution and the Implications for Life.

Osinski, G. R., 2003. Impact glasses in fallout suevites from the Ries impact structure, Germany: An analytical SEM study. Meteoritics & Planetary Science. 38**,** 1641-1667.

Osinski, G. R., 2007. Impact metamorphism of CaCO3-bearing sandstones at the Haughton structure, Canada. Meteoritics & Planetary Science. 42**,** 1945-1960.

Palumbo, A., Head, J., 2017. Impact cratering as the cause of climate change, atmospheric alteration, and late Noachian valley network formation on Mars: An assessment. 6th Mars Atmosphere Modeling and Observations Workshop, pp. 17-20.

Palumbo, A. M., Head, J. W., 2018. Impact cratering as a cause of climate change, surface alteration, and resurfacing during the early history of Mars. Meteoritics & Planetary Science. 53**,** 687-725.

Phinney, W., Simonds, C., Cochran, A., McGee, P., 1978. West clearwater, Quebec impact structure, part II: petrology. Lunar and Planetary Science Conference Proceedings, Vol. 9.

Pierazzo, E., Melosh, H., 2000. Melt production in oblique impacts. Icarus. 145**,** 252-261.

Pohl, J., Stoeffler, D., Gall, H. v., Ernstson, K., 1977. The Ries impact crater. Impact and explosion cratering: Planetary and terrestrial implications, pp. 343-404.

Poulet, F., et al., 2005. Phyllosilicates on Mars and implications for early Martian climate. Nature. 438**,** 623-627.

Rae, A., Collins, G., Grieve, R., Osinski, G., Morgan, J., 2017. Complex crater formation: Insights from combining observations of shock pressure distribution with numerical models at the West Clearwater Lake impact structure. Meteoritics & Planetary Science. 52**,** 1330-1350.

Robbins, S. J., Hynek, B. M., 2012. A new global database of Mars impact craters≥ 1 km: 2. Global crater properties and regional variations of the simple-to-complex transition diameter. Journal of Geophysical Research: Planets. 117.

Rocholl, A., Böhme, M., Gilg, H. A., Pohl, J., Schaltegger, U., Wijbrans, J., 2018. Comment on "A high-precision 40 Ar/39 Ar age for the Nördlinger Ries impact crater, Germany, and implications for the accurate dating of terrestrial impact events" by Schmieder et al.(Geochimica et Cosmochimica Acta 220 (2018) 146-157. Geochimica et Cosmochimica Acta.

Rosa, D. F., 2012. The sheet of impact melt at West Clearwater Lake, Northern Quebec. McGill University (Canada).

Schmieder, M., Kennedy, T., Jourdan, F., Buchner, E., Reimold, W. U., 2018. A high-precision 40Ar/39Ar age for the Nördlinger Ries impact crater, Germany, and implications for the accurate dating of terrestrial impact events. Geochimica et Cosmochimica Acta. 220**,** 146-157.

Schmieder, M., et al., 2015. New 40Ar/39Ar dating of the Clearwater Lake impact structures (Québec, Canada)–Not the binary asteroid impact it seems? Geochimica et Cosmochimica Acta. 148**,** 304-324.

Schultz, P. H., Mustard, J. F., 2004. Impact melts and glasses on Mars. Journal of Geophysical Research: Planets. 109.

Shipman, F., Gregson, V., Jones, A., 1971. A shock wave study of Coconino Sandstone. National Aeronautics and Space Administration.

Shoemaker, E. M., Kieffer, S. W., 1979. Guidebook to the geology of Meteor Crater, Arizona. Center for Meteorite Studies, Arizona State University.

Simonds, C., Phinney, W., McGee, P., Cochran, A., 1978. West Clearwater, Quebec impact structure. I-Field geology, structure and bulk chemistry. II-Petrology. Lunar and Planetary Science Conference Proceedings, Vol. 9, pp. 2633-2693.

Singleton, A. C., Osinski, G. R., McCAUSLAND, P. J., Moser, D. E., 2011. Shock-induced changes in density and porosity in shock-metamorphosed crystalline rocks, Haughton impact structure, Canada. Meteoritics & Planetary Science. 46**,** 1774-1786.

Smith, B., Srinivasan, S., Gomez-Heras, M., Basheer, P., Viles, H., 2011. Near-surface temperature cycling of stone and its implications for scales of surface deterioration. Geomorphology. 130**,** 76-82.

Smith, B., Warke, P., McGreevy, J., Kane, H., 2005. Salt-weathering simulations under hot desert conditions: agents of enlightenment or perpetuators of preconceptions? Geomorphology. 67**,** 211-227.

Sousa, L. M., del Río, L. M. S., Calleja, L., de Argandona, V. G. R., Rey, A. R., 2005. Influence of microfractures and porosity on the physico-mechanical properties and weathering of ornamental granites. Engineering Geology. 77**,** 153-168.

Squyres, S. W., et al., 2012. Ancient impact and aqueous processes at Endeavour Crater, Mars. Science. 336**,** 570-576.

Squyres, S. W., et al., 2009. Exploration of Victoria crater by the Mars rover Opportunity. Science. 324**,** 1058-1061.

Stöffler, D., Grieve, R., Fettes, D., Desmons, J., 2007. Impactites. Metamorphic rocks: A classification and glossary of terms, recommendations of the International Union of Geological Sciences. 82-92.

Stöffler, D., Hamann, C., Metzler, K., 2018. Shock metamorphism of planetary silicate rocks and sediments: Proposal for an updated classification system. Meteoritics & Planetary Science. 53**,** 5-49.

Tornabene, L. L., et al., 2013. An impact origin for hydrated silicates on Mars: A synthesis. Journal of Geophysical Research: Planets. 118**,** 994-1012.

Tuğrul, A., 2004. The effect of weathering on pore geometry and compressive strength of selected rock types from Turkey. Engineering Geology. 75**,** 215-227.

Tyburczy, J. A., Aherns, T., 1988. Dehydration kinetics of shocked serpentine. Lunar and planetary science conference proceedings, Vol. 18, pp. 435-441.

Viles, H., 2011 Weathering systems. In: D. S. Thomas, (Ed.), Arid zone geomorphology: process, form and change in drylands. John Wiley & Sons, pp. 85-101.

Viles, H., Ehlmann, B., Wilson, C. F., Cebula, T., Page, M., Bourke, M., 2010. Simulating weathering of basalt on Mars and Earth by thermal cycling. Geophys. Res. Lett. 37**,** L18201.

Viles, H., Goudie, A., 2007. Rapid salt weathering in the coastal Namib desert: implications for landscape development. Geomorphology. 85**,** 49-62.

Viles, H., Goudie, A., Grab, S., Lalley, J., 2011. The use of the Schmidt Hammer and Equotip for rock hardness assessment in geomorphology and heritage science: a comparative analysis. Earth Surface Processes and Landforms. 36**,** 320-333.

Viles, H., Messenzehl, K., Mayaud, J., Coombes, M., Bourke, M., 2018. Stress histories control rock-breakdown trajectories in arid environments. Geology. 46**,** 419-422.

Viles, H. A., 2005. Microclimate and weathering in the central Namib Desert, Namibia. Geomorphology. 67**,** 189-209.

Viles, H. A. J. N., 2014. Solar system: Cracking up on asteroids. 508**,** 190.

Warke, P., 2007. Complex weathering in drylands: implications of 'stress' history for rock debris breakdown and sediment release. Geomorphology. 85**,** 30-48.

Warke, P., Smith, B., 1998. Effects of direct and indirect heating on the validity of rock weathering simulation studies and durability tests. Geomorphology. 22**,** 347-357.

Weiss, D. K., Head, J. W., 2014. Ejecta mobility of layered ejecta craters on Mars: Assessing the influence of snow and ice deposits. Icarus. 233**,** 131-146.

Werner, S., Tanaka, K., 2011. Redefinition of the crater-density and absolute-age boundaries for the chronostratigraphic system of Mars. Icarus. 215**,** 603-607.

Wetherill, G., 1975. Late heavy bombardment of the moon and terrestrial planets. Lunar and Planetary Science Conference Proceedings, Vol. 6, pp. 1539-1561.

Williams, R., Robinson, D., 2001. Experimental frost weathering of sandstone by various combinations of salts. Earth surface processes and landforms. 26**,** 811-818.

Wolff-Boenisch, D., Gislason, S. R., Oelkers, E. H., 2006. The effect of crystallinity on dissolution rates and CO2 consumption capacity of silicates. Geochimica et Cosmochimica Acta. 70**,** 858-870.

Wright, S., 2013. Decompression Cracks in Altered Basalt Under Solid-State Shock Pressures: A New Macroscopic Shock Texture. LPI Contributions. 1737**,** 3049.

Zhu, L. p., Wang, J. c., Li, B. y., 2003. The impact of solar radiation upon rock weathering at low temperature: a laboratory study. Permafrost and Periglacial Processes. 14**,** 61-67.

Zolotov, M. Y., Mironenko, M. V., 2016. Chemical models for martian weathering profiles: Insights into formation of layered phyllosilicate and sulfate deposits. Icarus. 275**,** 203-220.